ISSN: 2331-1959 Volume 10, Number 2, April 2022

Scientific Research Publishing

Archaeological Discovery

ISSN: 2331-1959

https://www.scirp.org/journal/ad

Journal Editorial Board

ISSN Print: 2331-1959 ISSN Online: 2331-1967

https://www.scirp.org/journal/ad

Archaeological Discovery, 2022, 10, 69-113
https://www.scirp.org/journal/ad
ISSN Online: 2331-1967
ISSN Print: 2331-1959

Table of Contents

Volume 10 Number 2 April 2022

Archaeological Discovery (AD)
Journal Information

SUBSCRIPTIONS

The *Archaeological Discovery* (Online at Scientific Research Publishing, https://www.scirp.org/) is published quarterly by Scientific Research Publishing, Inc., USA.

Subscription rates:
Print: $39 per issue.
To subscribe, please contact Journals Subscriptions Department, E-mail: sub@scirp.org

SERVICES

Advertisements
Advertisement Sales Department, E-mail: service@scirp.org

Reprints (minimum quantity 100 copies)
Reprints Co-ordinator, Scientific Research Publishing, Inc., USA.
E-mail: sub@scirp.org

COPYRIGHT

PRODUCTION INFORMATION

For manuscripts that have been accepted for publication, please contact:
E-mail: ad@scirp.org

Archaeological Discovery, 2022, 10, 69-113
https://www.scirp.org/journal/ad
ISSN Online: 2331-1967
ISSN Print: 2331-1959

A Sluice Gate in Hezekiah's (Iron Age II) Aqueduct in Jerusalem: Archaeology, Architecture and the Petrochemical Setting of Its Micro and Macro Structures

Aryeh E. Shimron[1], Vitaly Gutkin[2], Vladimir Uvarov[2]

[1]Geological Survey of Israel (ret.), Jerusalem, Israel
[2]The Center for Nanoscience and Nanotechnology, The Hebrew University of Jerusalem, Jerusalem, Israel
Email: aeshimron@gmail.com

How to cite this paper: Shimron, A. E., Gutkin, V., & Uvarov, V. (2022). A Sluice Gate in Hezekiah's (Iron Age II) Aqueduct in Jerusalem: Archaeology, Architecture and the Petrochemical Setting of Its Micro and Macro Structures. *Archaeological Discovery, 10,* 69-113.
https://doi.org/10.4236/ad.2022.102004

Received: March 9, 2022
Accepted: April 26, 2022
Published: April 29, 2022

Abstract

As part of an important and unique engineering project to protect access to the only perennial source of water in Iron Age II Jerusalem, the engineers of the Israelite king Hezekiah (~715 - 686 BCE) excavated a 533-m-long-subterranean water conduit. His reign took place during a time when the Assyrian empire was consolidating its control of Palestine and Syria, and the threat to the city's only major water supply was acute and immediate. The aqueduct was constructed to transfer water from the Gihon spring, on the western flank of the Kidron Valley in NE Jerusalem, into the Siloam pool—a water reservoir built during the Middle Bronze II (MB II) Period and located inside the southeastern edge of the city. Hezekiah's engineers were well aware that such a diversion of water from the northern spring source south into the Siloam pool would lower the water level not only in the immediate environs of the Gihon spring cave but also from the main reservoirs and water conduits. It would thereby threaten the water sources supplying the city's religious and political heart. To deal with the problem a "device" to control water level in the new aqueduct and thereby also the spring environ was designed and eventually constructed about 71 m from the tunnel's southern exit. This was where the tunnel ceiling rises rapidly from a height of ~2 m and reaches almost 6 m at the tunnel exit. Two parameters were decisive in the design and choice of this location 1) a threat to the city's security and 2) the necessity to exercise control of the sluice system from without. Prior to tunnel inauguration four iron bolts > 8 cm in length and up to 1.2 cm wide, were hammered at about waist height through wood panels into which a wooden gate (the sluice) was fitted. A cable, probably woven of wool fiber, raised and lowered the gate. We re-

trieved and studied two of the four iron bolts and discovered that they are partially enveloped with accreted slivers of (apparently) cedar wood, now petrified to iron hydroxide. We have studied the bolts by SEM-EDS and XRD and were able to unravel a long history of oxidation of metallic iron during which the phases goethite, lepidocrocite, magnetite and lastly akaganeite crystallized—in that order. Collectively these species testify to corrosion of nails during a long history of a fluctuating, occasionally unique, chemical environment within the microcosm of the bolts and probably along the full length of the aqueduct. The external morphology of the bolts and the chemical composition of the metallic iron imply smelted low carbon wrought iron, hand-hammered into desired shapes. The ceiling above the nails is covered with plaster carrying organic matter and fragments of calcified organic fiber. Along nearby fracture zones pozzolanic mortar applications encircle hand-carved circular depressions, thereby collectively providing testimony to unique anthropogenic efforts invested specifically into this segment of the aqueduct.

Keywords

Jerusalem, Gihon Spring, Hezekiah's Iron Age II Tunnel, Ancient Plaster, Sluice Gate, Iron Bolts, Calcified Organic Fibers, Petrified Wood, Goethite, Lepidocrocite, Biomagnetite, Akaganeite, Fluctuating Chemical Milieu, Plastered Fracture Zones, Mamluke Plaster and Mortar, Shaft to Surface

1. Introduction

"*After all that Hezekiah had so faithfully done, Sennacherib king of Assyria came and invaded Judah. He laid siege to the fortified cities, thinking to conquer them for himself. When Hezekiah saw that Sennacherib had come and that he intended to make war on Jerusalem, he consulted with his officials and military staff about blocking off the water from the springs outside the city, and they helped him. A large force of men assembled, and they blocked all the springs and the stream that flowed through the land. 'Why should the kings of Assyria come and find plenty of water?' they said. Then he worked hard repairing all the broken sections of the wall and building towers on it. He built another wall outside that one and reinforced the supporting terraces of the City of David. He also made large numbers of weapons and shields*" (Chronicles 32: 1-5, 30). "*As for the other events of Hezekiah's reign, all his achievements and how he made the pool and the tunnel by which he brought water into the city, are they not written in the book of the annals of the kings of Judah?*" (Kings 20: 20).

Although the Old Testament can hardly be regarded as a reliable record of history, and in spite of claims that Hezekiah's tunnel was built several centuries after Hezekiah's reign, our contribution below shows that there is ample reason

to not question the bulk of the historicity of the biblical Chronicles and Kings narratives in the quotations above.

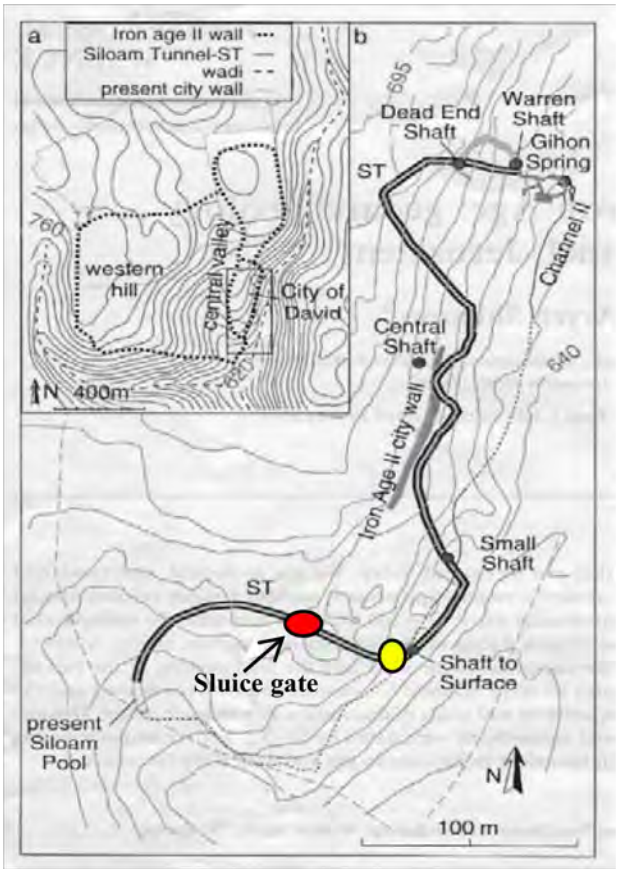

Figure 1. Overview map of Ancient Jerusalem showing the location of some of the main archaeological and architectural elements of the Gihon Spring waterworks. Note the confluence of Hezekiah's Aqueduct and Channel II (at ~2.4 m higher elevation) at the junction with the karstic Shaft to Surface (yellow). Contour interval 5m. ST refers to Siloam Tunnel, the original name for Hezekiah's Aqueduct—or tunnel. (Figure modified from Frumkin & Shimron, 2006).

Understanding the geography of the Jerusalem of the Old and New Testaments has been the focus of legions of scholars in many disciplines - historians, theologians, archaeologists, geologists and artists. In addition to the Temple Mount, the Gihon Spring (GS) waterworks has attracted considerable attention. The fact that GS (**Figure 1**), was the only perennial water source of significance in the city, determined the location and growth of the city's core, which was established during the Middle Bronze Age II (MB II) period, approximately 3800 years ago. The spring's water erupts from a fracture above a karstic aquifer (Amiel et al., 2010) at an elevation of ~635 m just beneath the city wall which is near the bottom of the western flank of the Kidron valley. The latter is a deep fault-line precipice that throughout history defined the eastern boundary of the city. Although protected by massive stone fortification since MB II the city and its waterworks lay dormant from about the 17th until the late 8th century BCE

(Reich & Shukrun, 1999, 2004) when the city reached its peak size.Whereas Palestine was now threatened by its neighbours from the NW, King Hezekiah's engineers planned and executed a complex engineering project – diverting the water from the GS and transferring the bulk of its waters into the Siloam Pool. The ancient pool, located within the walls at the SE edge of the city offered better protection to the GS waters then the spring environs. The king's engineers were well aware that such a diversion would significantly lower the water level in the northern water conduits and reservoirs (the cave beneath Warren's Shaft, the Round Chamber and Channel II, **Figures 2-4**). This would mean cutting off most of the water from the bulk of the city's population. In order to overcome such a potentially fatal threat a mechanism was needed that would allow the water level in the tunnel to be raised and lowered as and when needed. For this purpose two major precautionary steps were taken prior to allowing water flow through the tunnel: 1) the many voids in the newly exposed highly fractured and karstified tunnel walls were sealed with hydraulic plaster up to an average height (~2 m) of the tunnel ceiling (Vincent, 1911; Shimron et al., 1998, 2000) and 2) a movable damming source was constructed at a favourable location in the tunnel. This location had to be where the tunnel ceiling was high enough to allow such a blocking gate to be raised and lowered. In addition, the gate had to be controled from without the tunnel yet remain protected from enemies. We have been able to pin-point this location. It is situated near the confluence of the aqueduct with Channel II and the Shaft to Surface (**Figure 1**). Here all prerequisites are fulfilled and significantly, the site also displays powerful evidence of a long period of intense anthropologic activity.

2. Sampling and Analytical Procedures

Sampling of sediment flushed into the Hezekiah's Tunnel (HT) was carried out by the senior author with the assistance of Geological Survey of Israel geologist Dr. Moshe Shirav (ret.), and technician Shelomo Ashkenazy (ret). Sediment and wood chips from the rusted Nails 1 and 2 were scraped off with a stainless steel scalpel. As sampling small artifacts is a destructive process only a small amount (maximum 1/4 teaspoonful) of rusted iron and carbonate carapace could be removed from the oxidized surface of each nail for analyses.

X-ray powder diffraction measurements were performed by Dr. Vladimir Uvarov at the Hebrew University Nanolaboratory on the D8 Advance diffractometer with LynxEye-XE-T detector (Bruker AXS, Karlsruhe, Germany) operating in ID mode. Low-background quartz sample holders were carefully filled with the powder samples. XRD patterns within the range 6" to 86" 2Θ were recorded at room temperature using CuKα radiation (λ = 5418A) with following measurment conditions: tube voltage of 40 kV, tube current of 40 mA, step-scan mode with a step size of 0.02 2θ and counting time of 0.5 sec/step. Phase identification, crystallite size calculation and semi-quantitative analysis were performed using EVA 3.0 software. Rietveld refinement was performed using TOPAS 3.0 software.

Scanning Electron Microscope (SEM) analyses were carried out at the Hebrew University Nanolaboratory (The XPS Laboratory Unit for Nanocharacterization, The Harvey M. Krueger Center for Nanoscience and Nanotechnology) in Jerusalem) by Dr. Vitaly Gutkin (supervisor of the unit) and AES—the senior author. The scanning electron microscopy images were obtained using an FEI Quanta 200 ESEM in low-vacuum mode without any preliminary treatment and with a chamber pressure of 0.38 Torr and acceleration voltages of 15 - 20 kV. Elemental analyses were carried using EDX (Energy Dispersive X-Ray spectroscopy). Energy Dispersive X-Ray Spectroscopy is a chemical microanalysis technique used in conjunction with SEM. The EDX technique detects x-rays emitted from the sample during bombardment by an electron beam to characterize the elemental composition of the analyzed volume. SEM-EDS analyses are semi-quantitative in the sense that spot analyses also receive trace amounts of data from the surrounding matrix. All photos used in this manuscript, unless denoted otherwise, are SEM micrographs.

3. The Gihon Spring Waterworks: Geological Background, Archaeology, and Architecture

The present paper does not attempt to resolve the many controversial issues regarding the Gihon Spring—one of the focal areas of historical Jerusalem. Much has been learned about the site from archaeological excavations, geological mapping, and dating of ancient materials by archaeological and radiometric techniques (e.g. Warren & Conder, 1884; Vincent, 1911; Shiloh, 1981; Reich & Shukrun, 1999, 2000, 2004; Shimron et al., 1998; Frumkin et al., 2003, Frumkin & Shimron, 2006, Shimron & Frumkin, 2011) Detailed structural data show that the course of Hezekiah's Tunnel (HT, **Figure 5**) was engineered by man and excavated through mostly solid bedrock without a continuous natural karstic precursor and/or flowing stream to guide the tunnellers (Vincent, 1911: p. 21; Shimron et al., 2000; Shimron & Frumkin, 2011). A^{14}C age derived from a well-preserved fragment of wood retrieved from hydraulic plaster in the tunnel walls indicates that tunnel excavation took place between 822 - 796 BCE (Frumkin et al., 2003). The age of the wood implies tunnel construction took place ~100 years later than the biological age of the dated wood. This date confirms the approximate period of the Gihon Spring waterworks and consequently also most of the biblical narrative (above) regarding the construction of Hezekiah's tunnel. Claims that the HT was not built by Hezekiah but several centuries later (e.g. Rogerson & Davies, 1996) can be dismissed with confidence.

The Gihon Spring waterworks, in the past referred to as the Warren Shaft System, contains the following principal architectural and archaeological elements (**Table 1**, **Figure 2**, **Figure 3**): 1) The Upper Tunnel. This is the main subterranean entrance into the waterworks system from within the city's walls., It is dated to the Middle Bronze Period (MB II, ~1800 - 1700 BCE): 2) The lower (topographic) level reservoirs and conduits, including Channel II (also referred to as the Siloam

Channel) and the principal water basin, referred to as the Rock-cut Pool. Two stone blocking walls that prevented the Gihon Spring water from draining into the Kidron valley and the Spring and Pool Towers (Figure 2) with cyclopean masonry were constructed at about this time: 3) About 1000 years later during Iron Age II (IA II, ~800 - 700 BCE) the fortifications were again made accessible and returned to use, The Upper Tunnel was deepened and the excavation of the underlying short Lower Tunnel was carried out. During this time 4) the top of the Warren's Shaft (WS) which had already been discovered was purposely intersected and the karstic cave beneath it eventually became a secondary small water reservoir for drawing water up the WS. Soon thereafter 5) the excavation of Hezekiah's Aqueduct (a subterranean tunnel) was initiated.

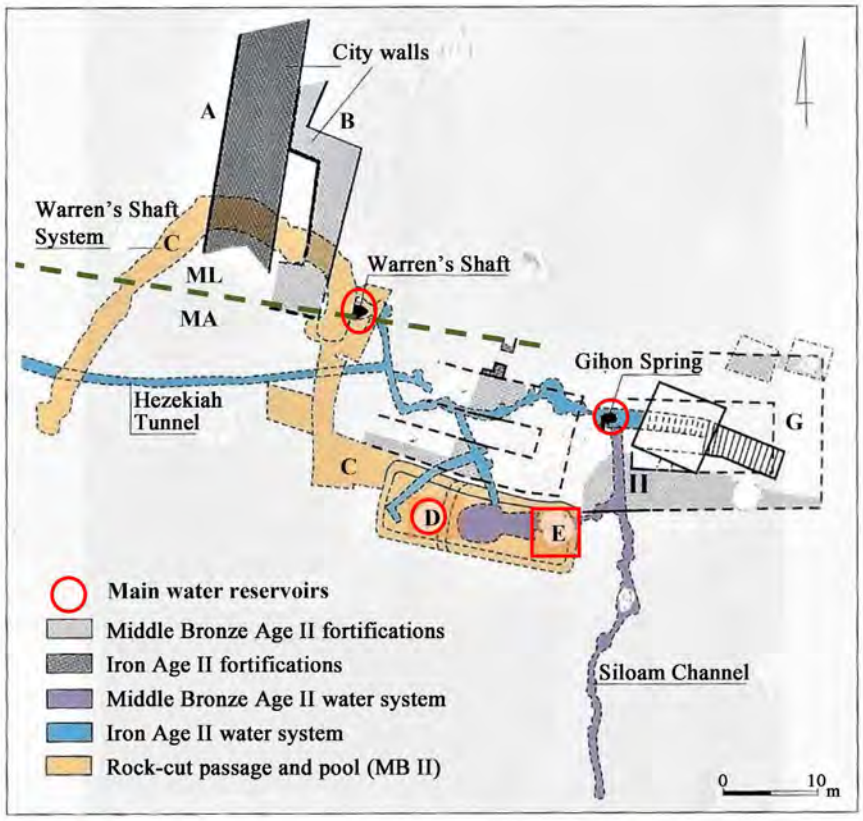

Figure 2. The plan view shows the principal communication tunnels, water conduits, reservoirs and fortifications of the Gihon Spring waterworks. A-Iron Age II (IA II-Israelite period) city wall, B-MB II (Canaanite) city wall, C-Upper Tunnel, D-Rock-cut Pool with the Round Chamber, E-Channel III, the main water feeder into the Round Chamber, II-(Siloam) Channel II, G-MB II fortification walls with cyclopean masonry. Principle elevation points: top of Warren's Shaft—647.2 m, bottom of Warren's Shaft—634.2 m, Hezekiah's Tunnel—634.9 m, Gihon Spring—635 m, Gihon Spring at fracture source—633 m, Channel II entrance—637.4 m, Floor of the Rock-cut Pool -637m. Marker line designates approximate contact between the upper soft-karstic Meleke (ML) and underlying hard Mizzi Ahmar (MA) formations. B, C, G, E and II are in major part Canaanite period (MB II) constructions. A, D and all blue-colored are Israelite (IA II) conduits and communication tunnels (Figure sources: Vincent, 1911 and with modifications after Reich, Avni and Winter, 1999).

We reason that the deepening of the Upper Tunnel was not only strategic but, in view of the approaching Assyrian threat urgent. The karstic cave adjoining the bottom of (WS) was accidentally discovered. In our view this probably took place during IA II as the GS was being reactivated (Shiloh, 1981, 1984; Reich & Shukrun, 2000) and Channel VI was being extended. The excavators followed a number of fractures from the spring cave westwards, then veered north along three N-S trending "leaky" wet fractures (**Figure 3**) which led them directly into the natural karstic cave and the bottom of the vertical WS shaft. We suggest that discovery and awareness of its potential sufficed to inspire Hezekiah's engineers to deepen the Upper Tunnel until the top of the WS was reached. The shaft eventually became a focal structure and conduit in the GS system, and provided access for fresh air to enter the HT now being excavated directly below. It also provided a channel through which rock rubble could be removed during the excavation taking place nearby. This eventually functioned as an important access route to the spring erupting almost directly below.

Sulley (1929), whose views were later taken up by Amiram (1976) and subsequently expanded by Gill (1991, 1994, 2012), proposed that "the curved S-shaped course of the tunnel indicated the former existence of a natural subterranean stream which carried water from the spring beneath the eastern hill emerging near where the present stream exit meets the Kidron Valley". Although published without any scientific data the idea was attractive. Gill (1991: p. 1469) in particular, attempted to provide a geological basis for the hypothesis. He summarized his views as follows: "A reexamination of the waterworks suggests that it was fashioned essentially by skillful enlargement of natural (karstic) dissolution channels and shafts and their integration into a functional water supply system". The idea which comprises precisely that "a reexamination and suggestions" without supportive structural geology data is convenient as it collectively accounts in simple terms how the main morphological elements (e.g. conduits, reservoirs and Hezekiah's aqueduct) of the GS waterworks were sculpted.

Vincent (1911) during his seminal work in the waterworks with the Parker mission during 1909-1911, searched but did not find any evidence which could provide support for Sully's hypothesis for the existence of a subterranean stream which shaped the S-shaped carving of the aqueduct. He dismissed the idea, in his words (1911, p. 21) "One thing is quite certain, and that we can be quite sure about, there is no spring (which shaped the tunnel) at all". And furthermore regarding the course of the tunnel "there is no question at all that these curves were intentionally made, even though they increased the length of the tunnel in the rock by nearly a third".

Figure 2 shows the boundary between the two main geological units which underlay Jerusalem, an upper unit called the Meleke Formation which, in major part, is a soft crumbly limestone underlain by the Mizzi Ahmar formation—a hard and compact, often dolomitic, limestone. Both formations contain many fractures and voids that pass into caves and vertical shafts and other morphological features caused by the dissolution of the bedrock. The Middle Bronze and

Iron Age engineers took advantage of these physiographic features and, where convenient, excavated along the fractures and karstic dissolution voids. What is clear, as already observed by Vincent over a hundred years ago and which we have shown in previous publications (e, g., Shimron et al., 1998, Shimron & Frumkin, 2011), is that in spite of the abundance of dissolution voids Hezekiah's Tunnel, with very few exceptions, does not follow these voids. Its morphology is not a product of karstic dissolution and it does not follow a fracture or a system of fractures or contacts between different geological units.

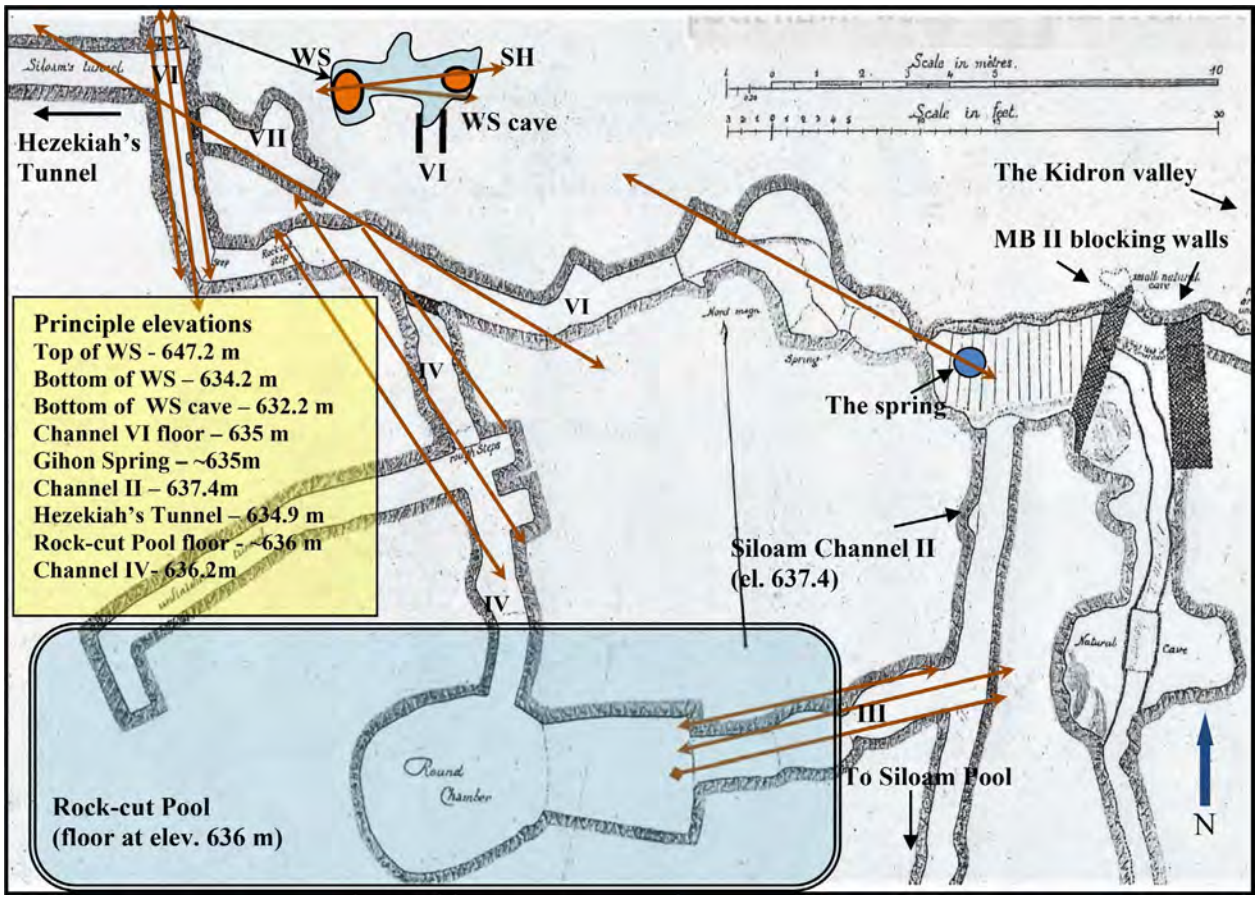

Figure 3. The figure shows the main conduits, reservoirs and linear structural features of the Gihon Spring waterworks. Fracture groups (arrows) trend 1) NW-SE (Channel IV, Channel VII, Gihon Spring cave, 2) N-S (westernmost segment of Channel VI, 3) E-W (Warren's Shaft and Warren's Shaft cave and Channel III. The excavation of Channels III, IV, VI and VII was much influenced by the location of these fracture zones. WS -Warren's Shaft, SH- karstic cave. Figure is modified after: Vincent (1911), Reich & Shukrun (2000, 2003), Shimron et al. (1998) and Frumkin & Shimron (2006).

Table 1. Man-made and natural installations of the Gihon Spring waterworks.

Installation	Function	Location	Elevations (from– to)	Age period
Gihon Spring	Sourced from a karstic aquifer	NE Jerusalem	~635 m	Quarternary
Upper Tunnel (UT)	Subterranean passage to the lower level water installations around the Gihon Spring	Entrance beneath MBII Stepped Wall	~661.91 m till 647.2 m at WS	MBII

Continued

Fortification towers	Rock walls with cyclopean masonry. Protected access to all GS installations	Encloses MBII installations		MBII
Rock-cut Pool	Main reservoir for Eastern Hill (east) Jerusalem. Tunnel III entered the pool close to its bottom at 637 m elevation.	~50 m SE of the spring	Floor of pool at 637 m	MBII
Channel II (Siloam Channel)	A near- surface rock-cut channel which carried water from the Gihon Spring into the Siloam Pool in southeast Jerusalem	Near-surface tunnel cut along Kidron Valley western flank	North entrance at 637.4 m	MBII
Tunnel III	Water conduit connecting Channel II with the Rock-cut Pool.	Branching from Channel II west	~637.3 m	MBII
Channel VI	Main water conduit from the GS into the WS cave and Hezekiah's Tunnel	GS area	~635 m	IA II
Lower Tunnel (LT)	Deepened segment of UT, intersects Warren's Shaft near its bottom termination	Connected with and directly beneath the Upper Tunnel	Bottoms at 647.2 m (at top of WS)	IA II
Warren's Shaft (WS)	Natural, vertical karstic dissolution shaft. Used to draw water from karstic cave beneath it during IA II		Top 647.9 Bottom 634.9 m	IA II
Warren's Shaft cave	Karstic cave beneath Warren's Shaft. Water- fed via Channel VI		632.12 (Cave floor)	Quarternary
Hezekiah's Tunnel (HT)	Subterranean aqueduct. HT provided secondary access and a secure supply of water to SE Jerusalem.		Entrance at ~635 m	~701 BCE
Sluice gate	Controled water level in HT aqueduct	71 m from S exit	~634.7 m	IA II
Siloam pool	Alternate water source for the Lower City. Acted as ritual pool since IA II		~ 605 m	MB II & later

How was the Water Level in the Waterworks Maintained and/or Elevated Once Hezekiah's Tunnel Was Activated

During MB II and prior to the Iron Age II excavation and inauguration of HT, water could be drawn from two main sources: 1) the Rock-cut pool (D and E **Figure 2**) whose floor lies ~1.4 m beneath the level of Channel II (Reich & Shukrun, 2003) at an alevation of ~636 m (~1 m above the level of the spring, **Figure 2**, **Figure 3**) and 2) from the spring cave (elevation 635 m), where water exits into Channel VI and, under certain conditions of high water into Channel II this at an elevation of 637.4 m. Access to water was also possible at the Siloam pool in the southeastern edge of the city (**Figure 1**) which, like the Rock-cut pool, was fed by the GS via Channel II. Alas, this could only be achieved when the spring was erupting (pulsating) at high pressure and water level rose to a sufficient height to reach the entrance into Channel II. After discovery of Warren's Shaft and its cave at the start of excavating HT, according to Vincent (1911: p. 16) " it was possible to draw water from the top of the shaft" and furthermore "before the opening of the aqueduct tunnel the hours when the spring flushed would

certainly cause the water to rise well up this shaft". We emphasize however, that this situation would have changed dramatically once the spring water was diverted down the HT conduit since the internal water circulation would have been disrupted since most water would now flow directly down Channel VI into HT and into the Siloam Pool. Relying on the pulsating eruptions of the spring to raise the water level a minimum of 2.4 m to feed Channel II was a risky proposition. Given the existing security threats, this could have potentially been fatal. Vincent labored with many of the tunnel issues but, to the best of our knowledge, nowhere does he attempt to address the latter in-depth. Other researchers of the waterworks have either disregarded the problem of water level entirely or attempted to deal with the dilemma as follows:

1) Vincent (1911: p. 16) after experimenting with drawing water up Warren's Shaft concluded that "it was quite possible to draw water from the top of the (Warren's) shaft". In addition, he observed that "before the initiation of the aqueduct tunnel the hours when the spring flushed would certainly cause the water to rise well up this shaft". One implication that can be drawn from this is that, once the HT was inaugurated, water in the WS cave would not have been at a high enough level to be drawn via the shaft. If so, then it is almost certain that water in the spring cave would have had difficulties in reaching the opening into Channel II which is at an elevation 2.4 m above the level of the spring.

2) Reich and Shukrun (2003: p. 77) postulated that no man-made installation was necessary in order to raise the spring's water level to a height necessary to feed Channel II and also the other installations since "the increase in flow during periodic water outbursts from the spring sufficed to raise the water level to the necessary height". They do emphasize that "the flow must have been erratic as the entrance into Channel II was 2.5 m above the spring cave".

3) Gill (1994) made a number of different, sometimes contradictory, proposals as to how the water issue was dealt with. For example (p. 64) he noted that to use the Warren's Shaft simultaneously with Hezekiah's Tunnel "it would have been necessary to do something to raise the water level in the water room at the bottom of Warren's Shaft. This could have been done easily by constructing a small dam somewhere along Hezekiah's tunnel". In another publication Gill (2012: p. 33) suggests that in order to solve the water level problem "it was essential to construct a pool to the east of the spring in which the spring outflow could rise spontaneously to the height of the channel's (Channel II) opening".

4) Regarding the usefulness of the shaft, Gill argues that "It could not, and hence did not, ever function as a water well because a bucket cannot be lowered freely through it due to its irregular walls and the elevation of its bottom is above the level of the spring". Gill disregarded Vincent's observations (above) made some 101 years earlier.

5) Meron (2002) suggested that in order to be able to draw water from Warren's Shaft "the spring water was raised to the desired level in the shaft by the tower walls that surrounded the source (Gihon Spring), acting as a dam (2002, p.

12)". This hypothesis is problematic because there is no physical connection between the Warren's Shaft cave and the Tower walls (Figure 2), which are well east of the spring cave.

All of the above investigators agree that diverting water down HT would have lowered its level in the Gihon water system to the extent that periodically it would have been necessary to raise it artificially. This was because water could not be drawn from their primary reservoirs. The Iron Age II engineers must have been well aware of the problem and that it would be necessary to control the water level in order to make the GS system functional as water conduits and reservoirs (Rock-cut Pool, Warren's Shaft and Channel II). We emphasize one of the solutions proposed by Gill (1994) that "a dam must have been constructed somewhere along Hezekiah's tunnel". We have searched for such a dam at what would be the ideal, perhaps only location for such a structure to be able to function effectively, and have found physical evidence for what may have been a movable blocking wall (sluice) at precisely such a place. We discuss our findings and related phenomena below.

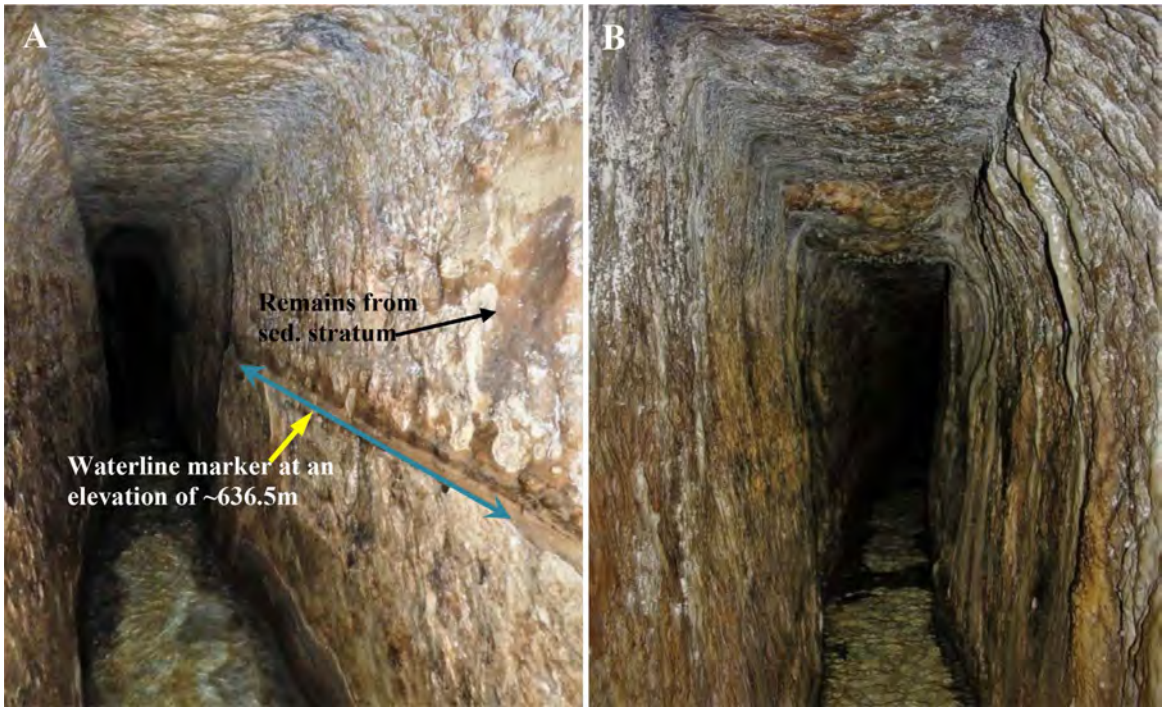

Figure 4. (A).Wall lamination (northern segment of tunnel) shows alternating silty and muddy layers (Figure 5). The dominant waterline level is at about 1.5 m above the tunnel floor which is at an elevation of ~635 m. In the absence of the frequently erratic ebb and flow (pulsating) nature of the spring this elevation would not suffice for the water to enter Channels II, the Rock-cut Pool (Figure 2, Figure 3) and fill the WS cave to a minimum level for drawing water. (B). Speleothems extending from dripstone on the tunnel ceiling. The innermost (oldest) laminae - dated to the 4th century BCE, cover 8th century BCE plaster and ancient waterlines such as seen in Figure 4(A).

4. The Sluice Gate: Choice of Location and Construction Architecture

As shown above, the King's engineers must have been aware that upon comple-

tion of the HT the diversion of most water flow from the GS southward into the Siloam pool would create an acute water problem in the northern heart of the city. The approaching Assyrian forces (Sennacherib besieged Jerusalem in ~701 BCE) would, in the dry semi-desert terrain, undoubtedly first secure their water sources—the Gihon Spring waterworks. The solution, we reason, was that, prior to inauguration of the tunnel, preparations were made to construct a dam-like installation that could, when needed, block waterflow toward the southern HT water outlet. Such blockage of the HT would raise the water level behind the dam but especially so in the WS cave, inside the spring cave and via Channel II also in the Rock-cut pool. As we show the ideal solution would be a movable (sluice) gate (**Figure 6**). The only feasible location in the aqueduct for the construction of such a gate, one from which water level could be controlled from a secure location—outside the tunnel, via a flexible cable connected to the sluice is ~71 m from the southern HT exit and ~40 m from the Shaft to Surface in the opposite ((SE) direction (**Figure 1**, **Figure 7**, **Figure 8**). The site was chosen precisely where the tunnel ceiling begins to rise sharply from an average height of <2 m culminating at an elevation of close to 6 m at the tunnel's southern exit. Where the ceiling rises to 3 m (floor to ceiling), four iron bolts, two on each side of the tunnel, were hammered, at about chest height, into the hard dolomitic limestone walls (**Figure 7**) thereby defining the precise location of the sluice gate. The sluice is located well within the walls of the city and the Shaft to Surface (the sluice gate cable exit) is some ~30 meters south from the city wall escarpment and beneath Channel II passing about 2 m above. This important junction of HT with its vertical dissolution shaft and Channel II directly above cannot be coincidental. A cable, apparently woven of wool (below), which led from the sluice gate to the Shaft to Surface had to be some ~50 m long in order to function. We

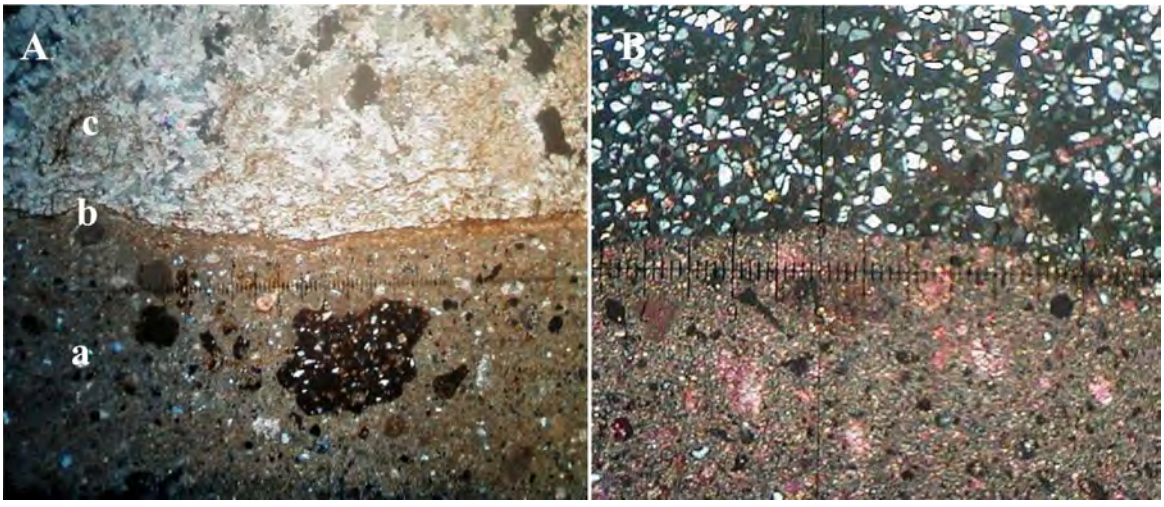

Figure 5. (A). The figure shows the oldest (Ancient) plaster (a) covered by a fine lamina of mudstone (b) followed by coarsely crystalline carbonate flowstone (c). The plaster constituents are mostly calcite (recarbonated lime), burned clays (amorphous black with white quartzose silt) and organic materials (isotropic, black); (B) Ancient plaster (lower half) covered by quartzose (white grains) siltstone. Black areas are burned clays. Optical microscope (transmitted polarized light). Scales are in mm, visible on photo B. The plaster is stained with alizarin red.

reason that it was operated from the surface outside the HT yet, if deemed necessary, it could easily have also functioned from the interior of Channel II via a subterranean Shaft to Surface connection.

Below we use the term sluice, or sluice gate, for a "movable gate constructed and used for controlling the level and flow of water". Traditionally it was made of wood (**Figure 6**), or more rarely as a metal barrier sliding in grooves that are set in the sides of a waterway. To the best of our knowledge no sluice gates have been recorded that predate the Roman ~1 - 2nd century CE Period (Schram, http://www.romanaqueducts.info). The oldest Iron Age structures referred to as sluice gates were found in the Judean Desert (Stager, 1976). Constructed to raise the level of water behind a stationary stone dam (photos provided in ref.), these structures are weirs rather then sluice gates. Consequently, if Hezekiah's Tunnel sluice ever functioned as a movable blocking wall, it may well be the oldest sluice gate on record.

Figure 6. An ancient (Middle Ages) sluice gate crossing a village stream in Morland, Cumbria UK. Note the hand crank on the upper left of the frame. Source: https://lindamphotos.wordpress.com.

4.1. The Sluice GateArea: Main Archaeological and Geological Features

The main morphological elements of our postulated sluice gate are shown in **Figure 9** and **Figure 10**, and additional structures in the immediate vicinity linked to the sluice workings in **Figures 11-18**. The materials and products of human craftsmanship we discovered include: 1) four rusted iron bolts symmetrically hammered into opposite (SE and NW) walls of the tunnel, on the ceiling above are present 2) three plastered fracture zones; 3) four rock-carved depressions three of which are ringed with pozzolanic mortar; 4) remains of calcified wool fibers embedded in the crust of plaster carrying fragments of organic carbon (soot) compounds; 5) a man-made truncation of a protrusion from the NW wall of which was replaced by a carved depression directly above the two bolts. We have also focused our efforts on; 6) examining the petrochemical compositions of the rusted nails, their well preserved metallic iron core, and a carapace

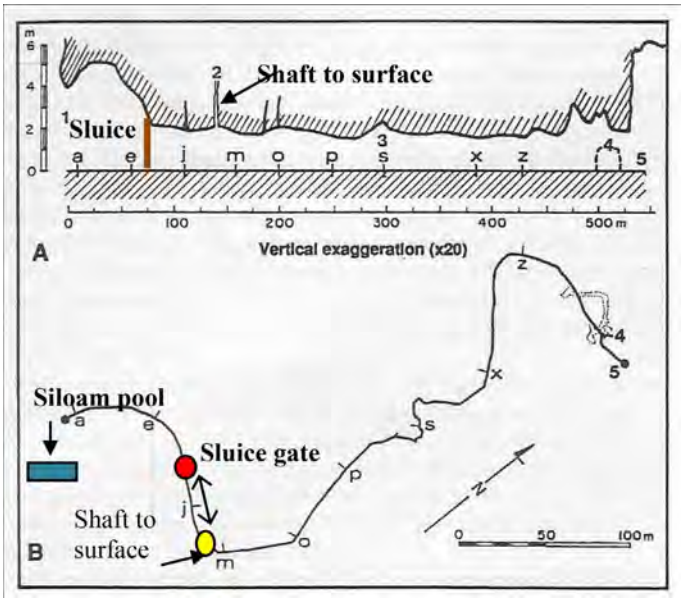

Figure 7. Longitudinal profile (A) and plan (B) of Hezekiah's Tunnel, modified after Vincent (1911) and Gill (1991). The letters show corresponding positions in the profile and plan views of the 533-m-long tunnel. Although highly variable the height of the ceiling is at ~1.7 - 2.0 m along most of its length.

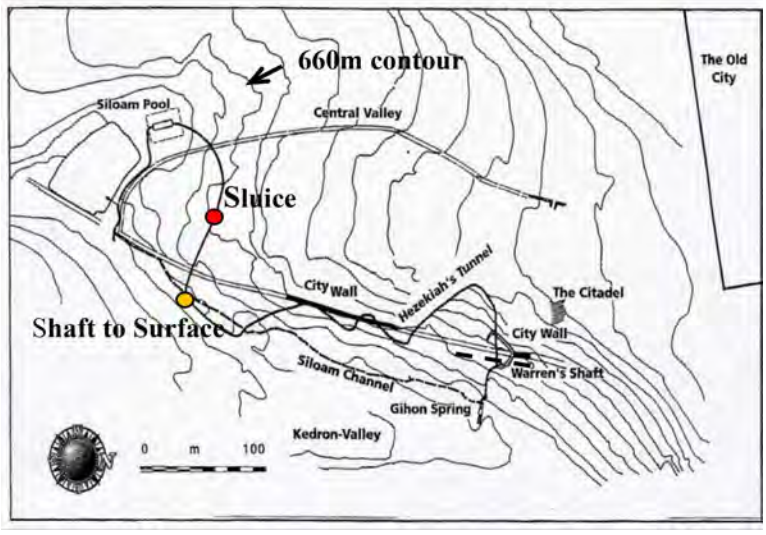

Figure 8.Topographic contours on the western slope of the Kidron Valley between the Gihon Spring and the southern outlet of Hezekiah's Tunnel showing the Iron Age II city wall and the two main water conduits—the MB II Siloam Channel and the IA II Hezekiah's Tunnel. Note that the Shaft to Surface is located at the junction of the two main water conduits located at different levels Channel II and Hezekiah's tunnel. Contour interval is 5 m, the sluice lies beneath the 660 m contour (Figure modified after Shiloh, 1984, **Figure 30**).

of four secondary iron species all enveloped within a veneer of petrified wood. Collectively, all these micro and macro materials and structural features are genetically linked with the design, construction and use of the sluice gate. We have utilized several lines of evidence in trying to estimate the approximate time of

sluice gate construction, they are as follows:

1) We have quoted from a number of previous studies thereby attempting to establish the necessity of constructing a movable dam-like structure that could control the water level in the newly constructed aqueduct. Considerable effort was devoted in the planning and execution of the tunnel, the latter included a good understanding of the tunnel's route, its bedrock materials and security issues. For example, in order to prevent the escape of water from HT via fractures and dissolution channels in the karstified limestone hundreds of kilograms of hydraulic plaster were applied to a thickness of ~6 cm and more to almost ceiling height (~2 m) along the full length of the channel. The latter was carried out prior to inauguration of the aqueduct.

2) Iron oxidation products. The iron bolts are oxidized to three species of iron hydroxides and one iron oxide. These products (including goethite, lepidocrocite, magnetite and akaganeite) combined with the late crystalline flowstone deposits, point to long periods of varying geochemical conditions not only in the confined environment of the iron bolts but most probably also along the full length of the tunnel.

3) Depositional laminae of fine sediment and water level markers (**Figure 4(A)**) can be seen along the tunnel walls, and in places they are covered by flowstone (**Figure 4(B)**). Frumkin et al. (2003) determined the age of the flowstone carbonate to be 4th century BCE using the U/Th method. Beneath the oldest (innermost) speleothem lamina we have discovered well preserved typical HT hydraulic plaster dated to the 8th century BCE. These dates indicate that some of the most pronounced and highest watermark levels were deposited between the 8th and 4th centuries BCE thereby confirming water level control already during this period.

4) The construction of the sluice gate and the application of plaster along the full length of the tunnel would have required a dry tunnel for carrying out this task. The most convenient time for this would have been prior to allowing water flow south towards the Siloam Pool - that is during Iron Age II.

4.2. Plastered Ceiling Fracture Zones, Carbonate Speleothem and Organic Fibers

About 71 m from the tunnel's southern exit four 0.5 to 1.5 m-wide heavily fractured black-stained zones cut in an approximately NNW-SSE direction across the tunnel ceiling. The fracture zones (Zones 1 - 3 in **Figure 11**, **Figure 15**, and **Figure 16**) are spread along the ceiling across an area of approximately 10 m and are covered with mm to cm-thick dark grey to black crusts composed of mortar and plaster. Because of their critical location and evidence of human activity we have studied these zones in considerable detail using SEM-EDS and XRD. We are able to conclude that there must be a link between the human efforts invested to the ceiling and the workings (e.g. four hammered bolts) and modifications in the tunnel-wall architecture almost directly beneath. Zone 1 is offset about 40 cm to the NE, Zone 2 is 1.4 m SW of Zone 1 and Zone 3 is 4.8 m SW of Zone 2.

The three zones marked by pronounced dark crusts, although similar in their overall appearance, the materials used differ in their chemical and mineral composition, perhaps in their functions and also periods in time. Chemical and mineral composition data of the materials used in the three zones are given in Table 2 and Table 3.

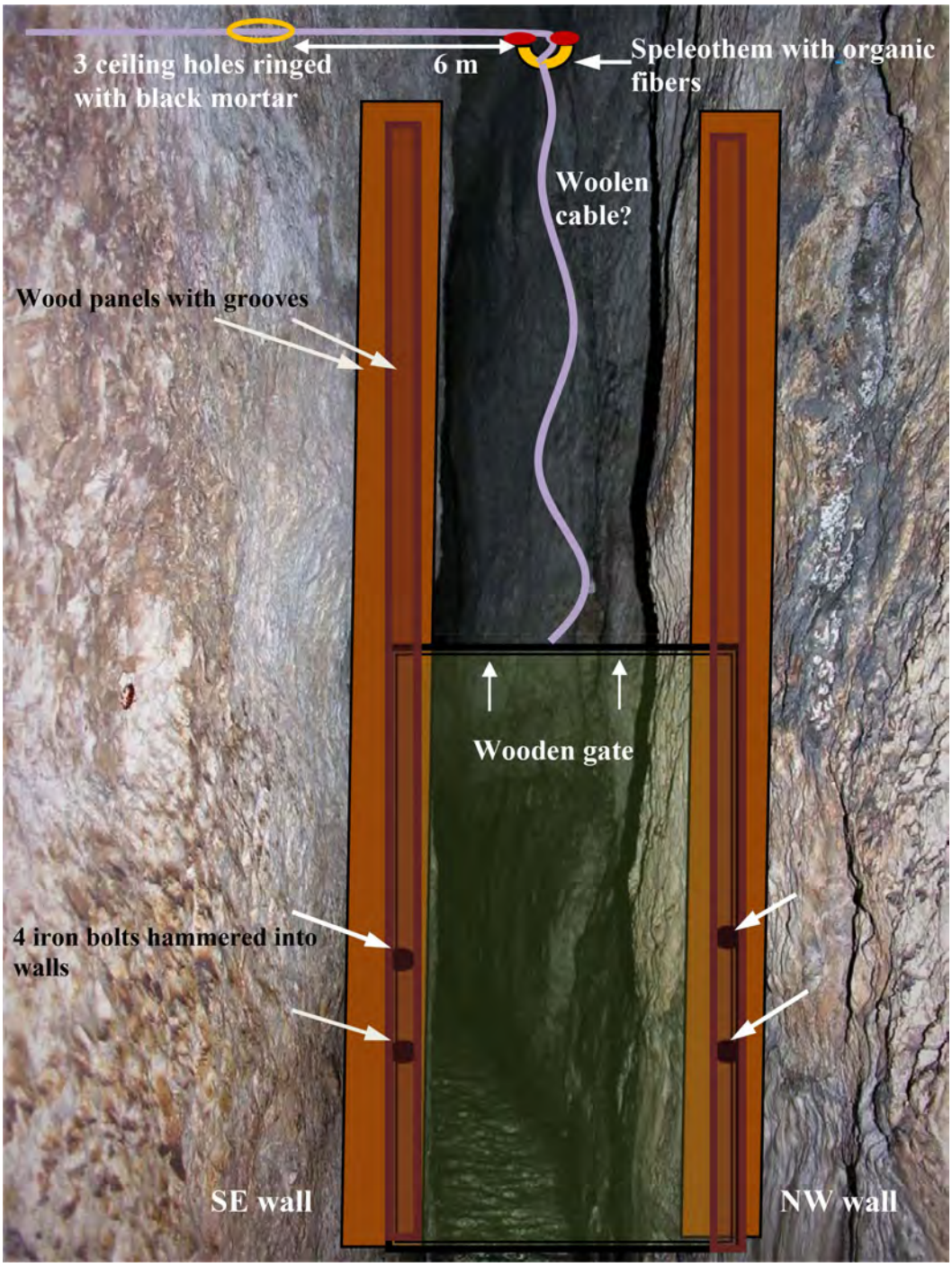

Figure 9. Postulated sluice gate in Hezekiah's tunnel, the figure is schematic and idealized. Architectural elements discovered at the site are (1) four iron bolts enveloped by slivers of petrified wood hammered on each side into the tunnel walls. Into the ceiling above (6 m to SW) three round holes ringed with layers of

black mortar were carved. In addition, the presence of what may be calcified wool fibers assimilated within ceiling crusts (details in text) justify our proposal that a cable woven of organic material passed through here and continued until it rose up through the karstic Shaft to Surface (Figure 7, Figure 8). View along the horizontal ceiling is toward the NE.

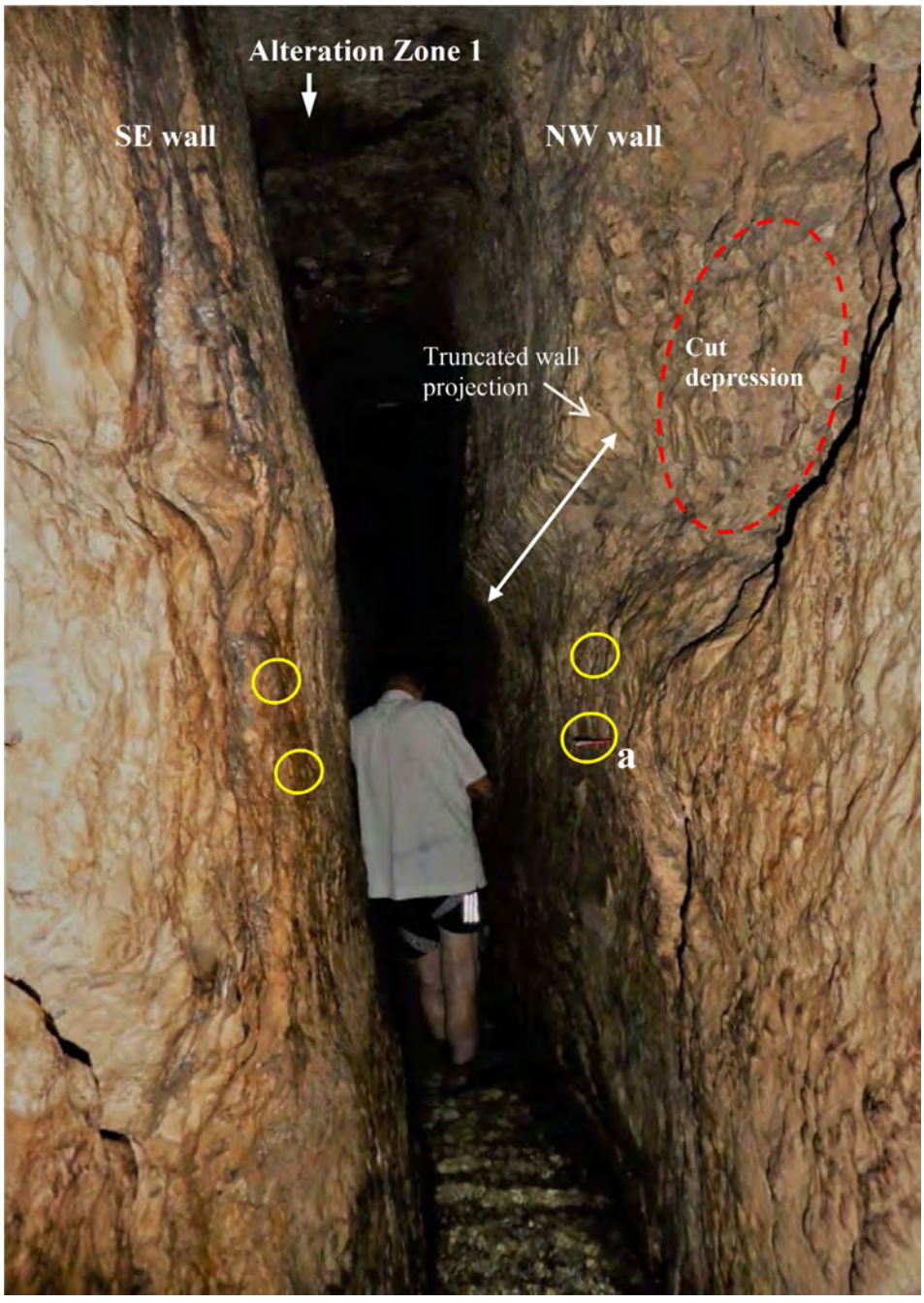

Figure 10. The sluice gate site. The locations of four nails hammered into walls are encircled. We inserted a pencil magnet into the void of Nail 1 at a, it is 135 cm above the tunnel floor. The white double-arrowed line delineates a wall projection abruptly terminated directly above the nails above which a man-made depression was hammered into the NW wall. Possibly a post Iron Age construction, it may have been prepared for the emplacement of the Siloam Inscription plaque which was eventually inserted into the wall near the tunnel's exit. Alteration Zone 1 is ~70 m from the tunnel's southern exit.

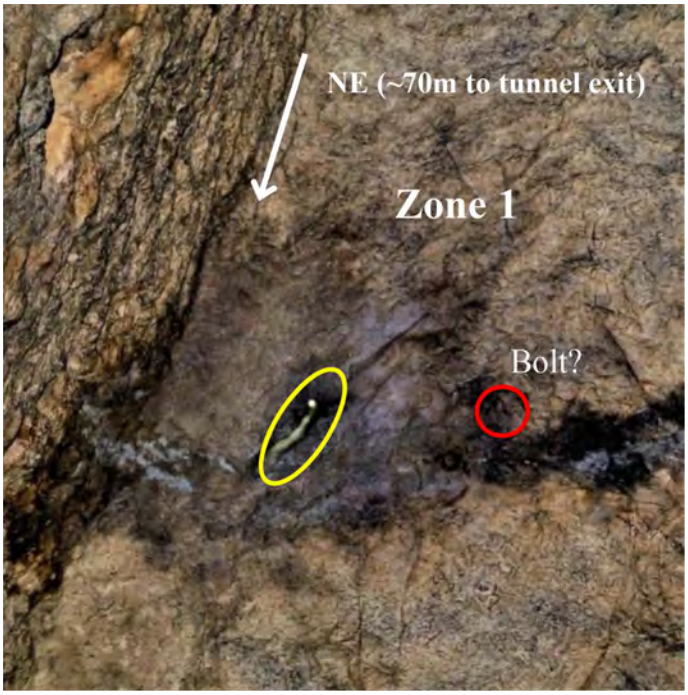

Figure 11. Zone 1. Encircled is a sausage-shaped carbonate speleothem (Figure 12, Figure 13 below) protruding from the interior of a fracture. Its presence implies that at least some of these fractures were wet and leaked solutions from overlying rocks. Protruding from the ceiling (encircled in red) is, what we interpret, a calcified bolt (Figure 13 below). The arrow lies along a NE trending horizontal contact line between the SE vertical wall (left side) and horizontal ceiling which contains the speleothem and bolt.

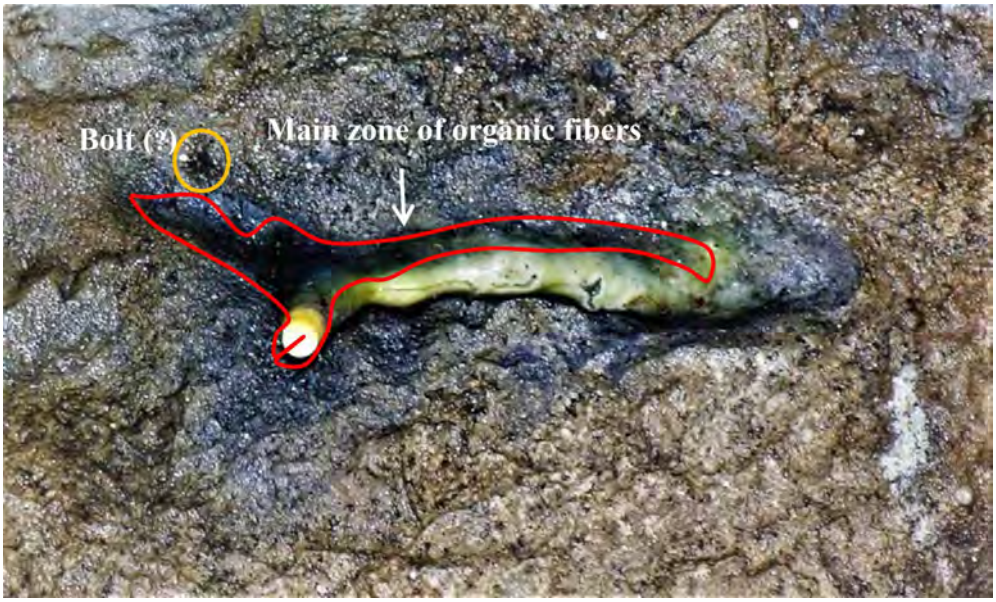

Figure 12. Detail of speleothem and its immediate surroundings. Much of the blue-colored zone, including the upper surface of the speleothem, is covered with a dark grey veneer of (recarbonated) lime plaster with soot particles. The red-outlined enclosure contains calcified organic fibers embedded in the surface crust. A color filter has highlighted the unusual organic-rich composition of the immediate area of the speleothem thus accentuating its uniqueness. (Table 2, Table 3 and Analyses for Zone 1).

Figure 13. Zone 1 ceiling speleothem (rotated into the orientation as seen in **Figure 11**). We attribute the distinctive deep blue coloring (filter enhanced) to the presence of organic carbon compounds contributed from soot and calcified fibers embedded in plaster. Note the presence of what is now a kind of calcified bolt (encircled yellow) emplaced in the ceiling near the speleothem.

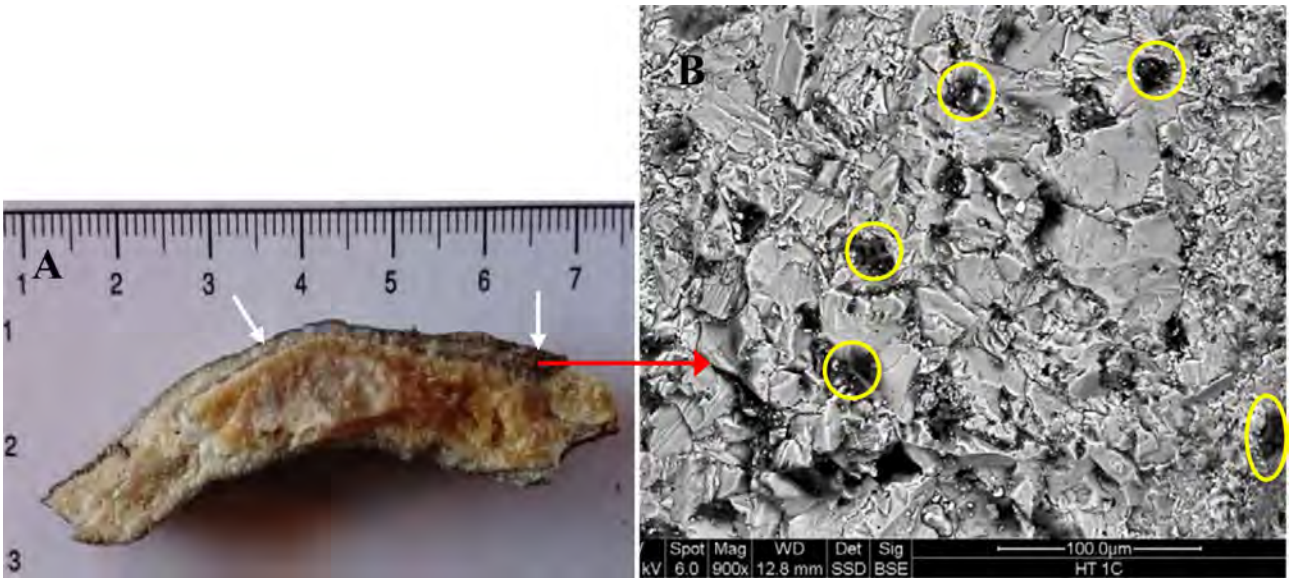

Figure 14. (A) Interior of the speleothem seen in **Figure 12**. Note the double layered ~0.3 mm-thick black carbonaceous crusts (arrows) covering the speleothem exterior (**Table 2**, HT1a, HT1-007). The outermost crust (magnified in 14B) has a concentration of carbon more than double that of the speleothem interior. Photo scale in cms. (B) Zone 1 general (SEM image) view of (recarbonated) lime plaster which covers most of Zone 1 ceiling. Black (encircled yellow) circular structures are organic carbon-rich particles. The circular grains are ~20 µm in size and are chemically compatible with soot. (See **Table 2**, **Table 3**, An. HT1C-011, 1C-014, 1C-015 and Gupta et al., 2019).

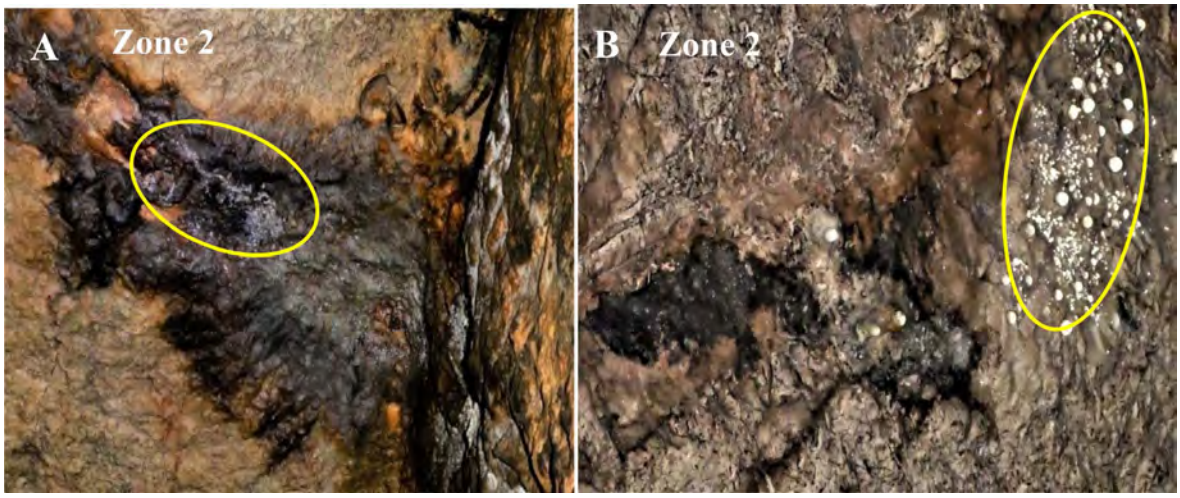

Figure 15. (A) Zone 2. Dark grey to black plastered ceiling carrying clusters of white spheres; (B) Cluster of spheres, some of these chemically zoned carbonate spheres have grown to immense size. Similar spherical structures are characteristic of fly or bottom ash produced during smelting of ore (see Table 2, Table 3, Analyses for Zone 2).

Figure 16. Tunnel ceiling, alteration Zone 3. Three hand-carved depressions (arrows) roughly encircled with a layer of black pozzolanic mortar. Another depression with a rust interior is present beneath (encircled red). (see Table 2, Table 3, Analyses for Zone 3).

Table 2. Chemistry of matrix aggregate and chosen materials in stained alteration Zones 1-3 on Hezekiah's tunnel ceiling. All values in volume %. Note table inserts for Ti, Cu and Zn in analyses for samples HT 5 and HT 5e.

Loc.	Samp.	Si	Al	Ca	Fe	Na	Mg	S	Cl	K	P	O	C
Zone 1	HT 1a	nd	nd	50.40	nd	nd	1.34	nd	nd	nd	nd	34.29	13.97
Zone 1	HT 1-003	nd	nd	65.73	nd	nd	0.47	nd	nd	nd	nd	25.32	8.48
Zone 1	HT 1-004	0.41	nd	75.68	nd	nd	0.40	0.51	nd	nd	0.20	15.94	6.86
Zone 1	HT 1-007	0.61	nd	31.72	nd	nd	1.01	nd	nd	nd	nd	47.11	19.55
Zone 1	HT1A-003	0.79	0.32	38.53	nd	0.45	0.71	0.48	0.29	0.58	0.18	31.19	26.49

Continued

Zone 1	HT1A-007	0.28	nd	58.94	nd	nd	0.69	0.64	nd	nd	0.24	27.33	11.89
Zone 1	HT1A-020	0.30	nd	43.46	nd	nd	0.94	0.51	nd	nd	0.17	37.76	16.87
Zone 1	HT1C-008	0.23	nd	48.71	nd	nd	0.98	nd	nd	nd	0.10	34.71	15.26
Zone 1	HT1C-010	0.33	nd	44.20	nd	nd	1.02	nd	nd	nd	0.12	35.92	18.14
Zone 1	HT1C-011	0.78	0.29	8.09	nd	3.42	0.48	0.98	3.69	2.25	0.07	16.28	63.68
Zone 1	HT1C-014	0.71	0.18	38.89	nd	0.52	1.09	0.22	0.40	0.53	0.17	32.44	24.84
Zone 1	HT1C- 015	1.09	0.35	33.99	nd	2.15	0.74	0.58	1.85	1.26	0.23	17.57	40.20
Zone 2	HT 2a	21.7	0.26	17.94	nd	nd	3.24	nd	nd	nd	nd	39.75	17.08
Zone 2	HT 2b	5.35	0.32	37.32	nd	nd	3.04	nd	nd	nd	nd	39.07	14.90
Zone 2	HT4-001	7.86	0.73	29.68	0.72	nd	2.95	0.62	nd	nd	nd	39.43	18.02
Zone 2	HT4-002	3.67	1.46	35.98	0.95	nd	1.05	0.52	nd	nd	nd	42.37	14.00
Zone 2	HT 4-003	0.87	nd	56.57	nd	nd	0.75	0.87	nd	nd	nd	32.53	8.41
Zone 2	HT4-006	5.17	1.01	31.75	0.81	nd	1.90	0.93	nd	0.48	1.11	38.38	18.46
Zone 2	HT3d	8.17	0.16	24.11	nd	nd	6.57	0.26	nd	nd	0.29	44.51	15.92
Zone 3	HT5A	1.58	0.49	12.80	73.93	nd	1.47	nd	nd	nd	nd	6.45	3.27
Zone 3	HT5-1	10.3	4.37	27.18	2.58	nd	1.87	0.29	nd	nd	0.19	42.21	10.03
Zone 3	HT 5	3.63	1.06	3.45	28.68	Ti% 29.2	1.59	nd	nd	nd	nd	29.18	3.63
Zone 3	HT 5a	1.54	0.63	6.30	59.56	nd	0.94	22.9	nd	nd	nd	4.38	3.75
Zone 3	HT 5b	1.27	0.37	5.97	62.10	nd	0.54	21. 9	nd	nd	nd	3.55	4.30
Zone 3	HT 5c	1.73	0.65	19.67	70.31	nd	0.82	nd	nd	nd	nd	4.19	2.62
Zone 3	HT 5e	1.19	0.53	16.70	nd	nd	6.44	0.78	0.61	nd	nd	31.25	10.36
Zone 3	HT 5e	Cu = 5.04%, Zn = 27.09%											

Table 3. Explanations to **Table 1** and XRD analyses.

Number	Location	Material analyzed	XRD analysis
HT 1a	Zone 1		Calcite
HT 1-003		Black 0.3mm thick crust covering sausage- shaped speleothem	Calcite
HT 1-004	Zone 1	Cross-section across cluster of spongy fibers	
HT 1-007	Zone 1	Micro-laminated speleothem (interior of speleothem above)	Calcite
HT1A-003	Zone 1	White protrusion from speleothem, average composition of matrix, include plates and fibers	
HT1A-007	Zone 1	White protrusion of speleothem, detail on cross-section of spongy fiber	
HT1A-020	Zone 1	Detail on twinned crystalline carbonate	
HT1C-008	Zone 1	Speleothem, interior in cross section, coarse crystalline calcite	
HT1C-010	Zone 1	Outer black crust in speleothem cross section interior. Detail on calcite plates of lime plaster	

Continued

HT1C-011	Zone 1	Detail on near surface black organic matter. Probably soot particles	
HT1C-014	Zone 1	As above, lime plaster with black organic matter. Soot particles	
HT1C-015	Zone 1	Detail on black organic carbon nodule	
HT 2a	Zone 2	Granular matrix, recarbonated lime, dolomite, quartz plaster	Calcite, dolomite, aragonite, quartz
HT 1a	Zone 2	Granular matrix, clasts 5 - 10 μm in size	
HT 3d	Zone 2	Lime plaster above laminae of flowstone	
HT 4-001	Zone 2	General, granular heterogeneous texture. Mortar-like fabric.	
HT4-002	Zone 2	Zoned sphere ~3mm diameter, Apparently bottom ash added to prepare pozzolanic plaster.	
HT 4-003	Zone 2	Calcareous spheroids, possibly bottom ash	
HT 4-006	Zone 2	Coarse granular mortar, general composition	
HT 5A	Zone 3	Metallic fragment, vesicular FeCa phase, as HT 5c	
HT 5-1	Zone 3	Hydraulic plaster layer	Calcite, quartz, vaterite, gehlenite and anorthite in mortar aggregate.
HT 5	Zone 3	Grey-black mortar aggregate. Analysis on ilmenite nodule.	
HT 5a	Zone 3	Pyrite, cube	
HT 5b	Zone 3	Pyrite, cube	
HT 5c	Zone 3	Metallic, vesicular, FeCa phase, chips ~60um	
HT 5e	Zone 3	Metallic grain, high ZnCu phase	Aurichalcite (?)

Zone 1. SEM-EDS and XRD analyses (Analyses HT1, HT 1a, HT 1-003, HT 1-007) show that the grey-black colored ceiling comprising Zone 1 consists mostly of fine layers of lime plaster. Within the core of this deeply miscolored area of Zone 1 (**Figure 12**, **Figure 13**) lies, horizontally rooted into the ceiling, a conspicuous sausage-shaped carbonate speleothem. XRD analyses of the flowstone show that it is calcite whereas its black surface crust (**Figure 14(a)**, **Figure 14(b)**) are laminae of recarbonated lime plaster carrying embedded circular to oval-shaped particles of organic carbon containing small amounts of Si, Al, Na, Cl, S, P and K (**Table 2**, An. HT1C-011, -014, 015). The particles are soot from burning fuel for oil lamps and/or torches which provided light for workers (see Sebela et al., 2015; Gupta, et al., 2019). Additional SEM images and analyses of the crust reveal the presence of an unusual fibrous carbonate (**Figures 17-19**, An. **Table 2**, HT 1-004) embedded into the outermost surface of the speleothem and its immediate surroundings. Based on its microfabric we have reason to interpret the fibrous materials to constitute calcified wool (hair) fibers. We note that the upper-outer surface of many clustered fibers lies within a single planar surface that appears to be polished (**Figure 18**, **Figure 19**). The collective evidence indicates that most of the organic materials adhering to and assimilated

within Zone 1 plaster and speleothem are due to extensive anthropogenic activity in the environs of the sluice gate. This plaster was applied during a different period in time than the mortars of Zones 2 and 3 and may well be contemporaneous with the construction of the sluice gate. Photographic filters were used on the SEM image (**Figure 13**) to highlight the stained surface crust in the immediate environs of the speleothem.

Zone 2. The surface crust of Zone 2 consists of a base layer of carbonate flowstone contributed by surface moisture, which penetrated into the tunnel through a much fractured ceiling (**Figures 11-16**). The flowstone layer is covered with a layer of coarse plaster, or mortar, made of lime with an aggregate of quartzose silt with varying amounts of added clayey and ferruginous components (**Table 2**, **Table 3**, An. for Zone 2 and **Figure 15**). The aggregate matrix is fragmental and shows moderate concentrations of Si with varying values in Al, Fe and traces of S and P. XRD analyses show the presence of calcite (recarbonated lime) with quartz, dolomite, aragonite, ankerite and traces of gypsum. Notable in this zone are clusters of carbonate spheroids, individual spheroids are chemically zoned showing trace amounts of Si, Al, Mg, S, and Fe (**Figure 15(a)**, **Figure 15(b)** and **Table 2**, An. HT 4-002, 4-003). The spheroids, whose size ranges from microns to ~3 mm in diameter, imply contributions from an "atypical" fly or bottom ash, possibly a combustion residuum from the smelting of iron, probably in the immediate vicinity (proximity of water) of the Gihon waterworks. Bottom ash (spheroids) was apparently added to the plaster as a pozzolan, which made it impermeable to the wet conditions such as were encountered in this much fractured area of the aqueduct. We cannot at this time conclude if Zone 2 and Zone 3 pozzolanic mortars are contemporaneous having served different functions, or are applications from different periods in time.

Zone 3.What we refer to as the "Mamluke zone" (**Figure 16**) consists of three hand-carved round depressions ~5 cm deep and ~5 cm diameter carved into the hard dolomitic limestone ceiling. A fourth depression, beneath the above, is heavily coated with brown rust in its interior. The depressions are ringed by fine layers of black hydraulic mortar thereby marking them as important features in the local architectural setting. The mortar is unique and differs from the common (8^{th} century BCE) hydraulic plaster still evidenced along most of the aqueduct. The mortar is characterized by high concentrations of the elements Ca, Fe, Mg and S (**Table 2**, **Table 3**, An. HT5A - HT5e) which we attribute to the presence of ferruginous pyritic iron ore slag, FeCa and ZnCu species, traces of high temperature calc-silicates such as gehlenite and anorthite and rare charred wood chips added to what is now a recarbonated lime base (**Table 2**, An. HT 5 –HT5e), A similar black plaster characterizes a number of wall repairs and karstic voids along the tunnel and a similar mortar also covers walls constructed to block access of water into a number of unused conduits in the area of the spring.We have dated a fragment of charred wood retrieved from the black mortar and obtained an ^{14}C age of 605 ± 65 yr.BP (Frumkin et al., 2003, Frumkin & Shimron, 2006). Based on the above age we have here documented what con-

stituted an important period of intense Mamluke Period activity in the vicinity of the spring and, as we show, also at what may have functioned as a sluice gate since Iron Age II. The mortar aggregate with remains of slag, fragments of base metals and pyritic iron ore collectively with bottom ash, suggest a hitherto undiscovered presence of a smelting furnace in the proximity of the Gihon waterworks.

4.3. Sluice Gate Walls with Hammered Bolts Underneath Zone 1

Our model of what the HT hypothetical sluice gate may have looked like (Figure 9) prior to its obliteration by physical elements and time is based on a number of observations and field discoveries some of which are depicted and mentioned above. Comparing the figures one can easily observe that the symmetrical disposition of the structural elements as postulated in Figure 9 is demolished by the obvious asymmetry when viewing the two walls that held the sluice in Figure 10. The SE wall has a relatively smooth vertical face which could have supported part of a wooden frame holding the SE flank of the sluice. The NW, wall on the other hand, exhibits a rough morphology and could not have held the kind of

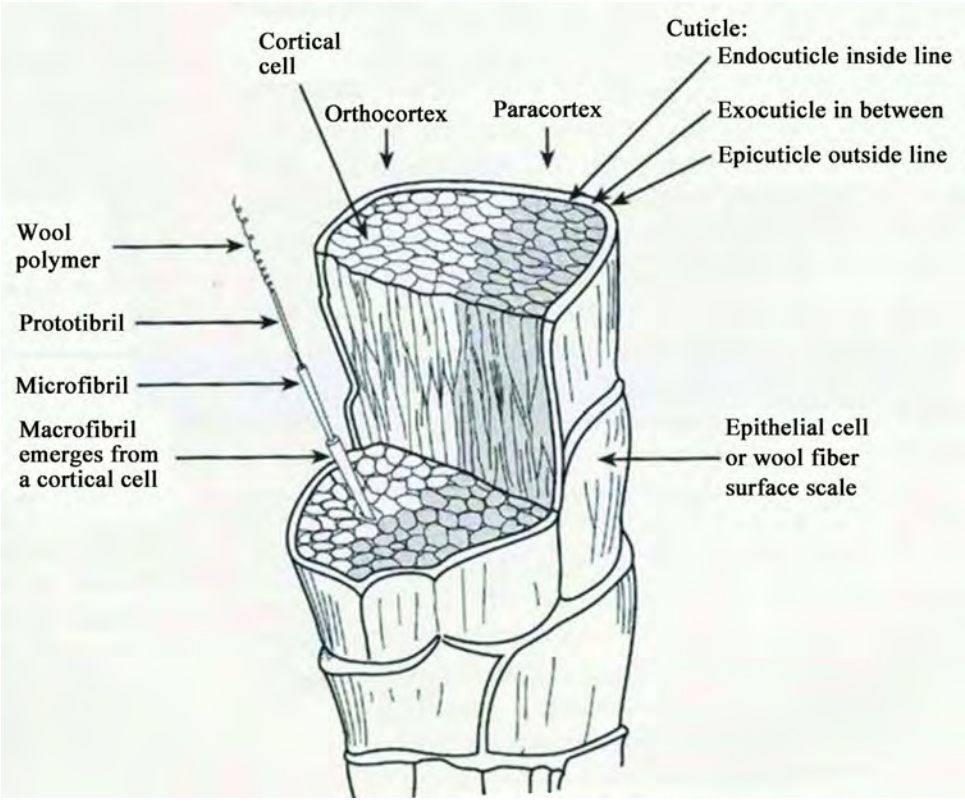

Figure 17. Cross-sectional and longitudinal view of a wool fiber showing its most important micro-structural features. The outer part of the fiber stem forms the cuticle. This segment consists of thin, flat-curving sheets that overlap one another like fish scales. The scales can be several layers thick. Inward the cuticle is followed by the epidermis and the cortex which contains keratin and melanin in rod-like fibrous cells twisted together like a rope. Finally, the core of the hair is the medulla which forms the soft area at the center. Source: http://textileaid.blogspot.com/2013/07/wool-fiber-chemical-composition-of-wool.html.

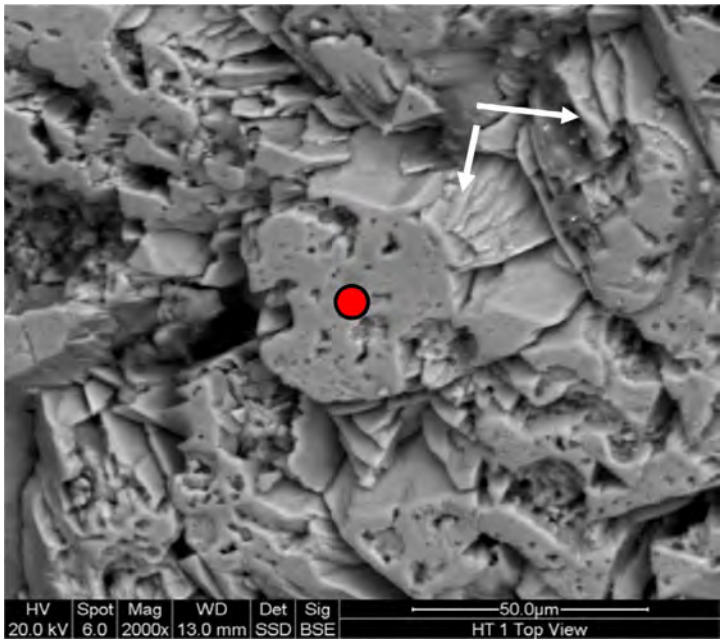

Figure 18. Zone 1 grey crust showing cross-sectional and longitudinal views of what we interpret to comprise a batch of calcified organic fibers. The curving cuticle sheets of two fibers (white arrows) are seen, the planar top faces comprise the cortex of the fiber cluster. Mean individual fiber diameter is ~30 µm, fairly typical for mammalian hair fibers. Note the difference in the chemical composition of the fibers which contain an abundance of trace elements (red marker, **Table 2**, An. HT1-004,) and the platy carbonate substratum seen in **Figure 19** (**Table 2**, An. HT 1a). It is significant that the frequently fibrous carbonate aragonite was not identified by XRD analyses amongst the carbonates of Zone 1.

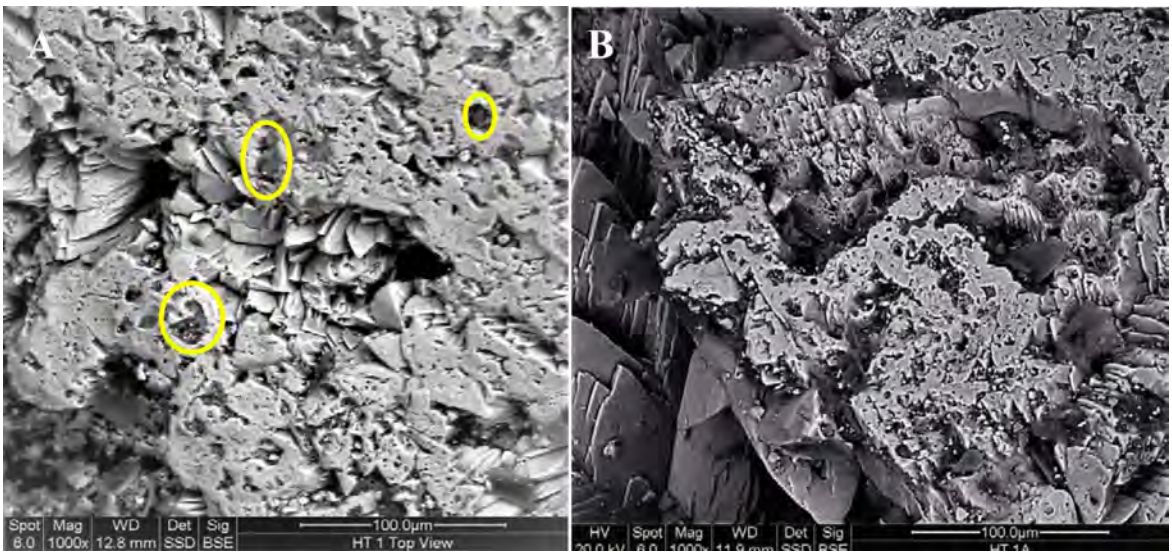

Figure 19. (A) Zone 1 grey crust. Detail cross-sectional view of what we interpret to be calcified fibers above a substratum of platy carbonate. Embedded in the fibers' surface (encircled yellow) are black particle of soot (see **Figure 14(B)** and **Table 2**, An. HT1C-011, 1C-014, 1c-015). Note that the outer-top faces of the fibers lie on the same planar surface that appears to be well polished. We have no geological explanation for this feature which may be the result of attrition between a moving and stationary surface. (B) Planar, polished-like surface of calcareous fibers above a platy carbonate base. The surface is dotted with black particles of soot. The fibrous micro- layer is ~ 15 - 20 µm thick.

flat wooden frame depicted in **Figure 9**. Almost directly above the two bolts hammered into the NW wall the edge of the projecting upper wall was truncated and a rough elliptical-shaped depression ~15 cm deep and up to 40 cm long was carved into the wall. We can only speculate regarding the period and objective of what must be a "late stage" modification of the NW wall surface. We hypothesise that this surface was being prepared to receive the emplacement of the well known Hezekiah's tunnel inscription tablet (Frumkin et al., 2003). Should this indeed have been the objective it was obviously not carried out as the surface does not appear to have been completed and the inscription tablet was eventually inserted into the SE wall within a few meters of the tunnel's southern exit.We point out that a similar preparation for the emplacement of a tablet was done near the junction of Channel IV and the Rock-cut Pool (Vincent, 1911; Reich & Shukrun, 2003, **Figure 3**). Most biblical scholars have ccepted the interpretation that the Siloam inscription celebrates the meeting of two teams upon completion of HT excavation however we emphasize that this acceptance is not universal and a much later date for both the carving of the tunnel and emplacement of the inscription has also been proposed (see Rogerson & Davies, 1996; Norin, 1998 for a full discussion). As a possible alternative explanation for the late modifications on the NW wall of the sluice we suggest a possible link with Mamluke period activity we described for alteration Zones 2 and 3 above.

5. Gihon Spring: Chemistry of Water

We show below in **Table 4** chemical data for water erupting from the Gihon Spring aquifer. The data are for the period Nov.2004 - Jan.2005, they show the variation in composition for some contaminating anions in the Gihon Spring water. The pH level for the above period, given by the Gihon (Jerusalem) water company is 7.1, and as 7.3 for 2019. It is probable that the pH level of the Gihon Spring fluctuated considerably in the distal past as shown by the Fe-oxidation products on the nails (below). The 7.1 value is low especially for a limestone terrain where pH values would under normal circumstances be similar to that of groundwater flowing through limestone strata where values are as high as 8.5. The 7.1 pH of the Gihon waters for the year 2010 (Water Commission Hydrological Service, 1970-1998 report) is similar to ground water flowing through a sandstone rather than a limestone terrain. We point out that surface strata covering the walls of HT are very much enriched in quartzose silt (**Figure 5(B)**), a contribution from the Gihon Spring aquifer. A quartzose environment with standing water will result in a lower than "normal (pH 7), an "acid" environment. According to WHO the chloride concentration in chlorinated drinking water is about 250 mg/litre. Chloride concentrations between 1 and 100 ppm can be viewed as very high, that is about double maximum values for a fresh water spring (100 ppm = 0.01%, 1 ppm = 1 mg/l).We note that Amiel et al. (2010) identified in the Gihon waters, among others also fecal coliform bacterial pollutants. A fecal coliform is a facultatively anaerobic, rod-shaped, gram-negative, non-sporulating bacterium.

Table 4. Chemical composition of the Gihon Spring water ((modified after Amiel et al., 2010).

	16/11 2004	22/11 2034	30/11 2004	2/1 2005	3/1 2005	10/1 2005	26/1 2005
Anion	mg/l	mg/l	mg/l	mg/l	mg/l	mg/l	mg/l
F^-	bdl	bdl	bdl	bdl	bdl	bdl	bdl
Cl^-	203	210	204	217	208	183	200
Br^-	1	0.5	1.1	1.8	0.9	0.18	0.3
NO_3^-	113	117	111	111	104	102	102
PO_4^{3-}	0.3	0.2	0.1	bdl	bdl	0.8	0.4
SO_4^{2-}	73	75	76	78	76	73	72
HCO_3^-	191	188	188	327	340	291	230

bdl—below detection limit.

6. The Sluice Gate Bolts: Accreted Wood, Iron Metallurgy, Petrochemistry and Significance of the Oxidation Products

Two of the four nails (shown in Figure 20, Figure 21, Table 5, Table 6) were analyzed by XRD and SEM-EDS with the hope of shedding light on the possible construction age of the sluice gate. The former provides us, within certain limits, with the mineral composition of the nails (Figure 22), the latter provides us with semi-quantitative chemical analyses of the metallic iron and its secondary constituents. What remains of Nail 1 is ~8 cm long, the nail is tapered, bent, and the head appears to be broken off. What remains of Nail 2 is ~5 cm long. It is slightly tapered and its narrow end and head are bent and broken. What comprises the present head is rosette-shaped showing radiating (by hammer impact?) fractures. We reason that since the nails were hammered through wood panels once the latter disappeared, either by removal or due to erosion, the remaining protrusions were hammered into the wall at which time they were bent and partially broken. The head of Nail 2 is covered with a white crust containing, in addition to the main calcite constituent, also aragonite, gypsum, quartz and ankerite. The surface morphology of the nails shows a rough – pitted outer surface suggesting that the nails are made of wrought iron (see below) which had to be hammered into the desired shape

6.1. Iron of the Nails

In a study of ancient weapons, tools and other artifacts Pense (2000) showed that there was little change in iron manufacturing from about 1000 BCE to 1000 CE, a time span of ~2000 years. The earliest type of iron produced is wrought iron, as it was easier to produce than cast iron and steel it is the most common iron in early history and thus the iron of most ancient artifacts. It derives its name from the process by which it was made, the raw iron was literally "wrought" by hammering

and shaping when hot. Wrought iron was simply made without the addition of a reducing agent like charcoal which characterizes other modes of iron manufacture. It was smelted in a bloomery where the iron is separated from its ore as a spongy bloom below its melting temperature. The iron bloom was then consolidated and shaped with a hammer to produce wrought iron. With respect to cast

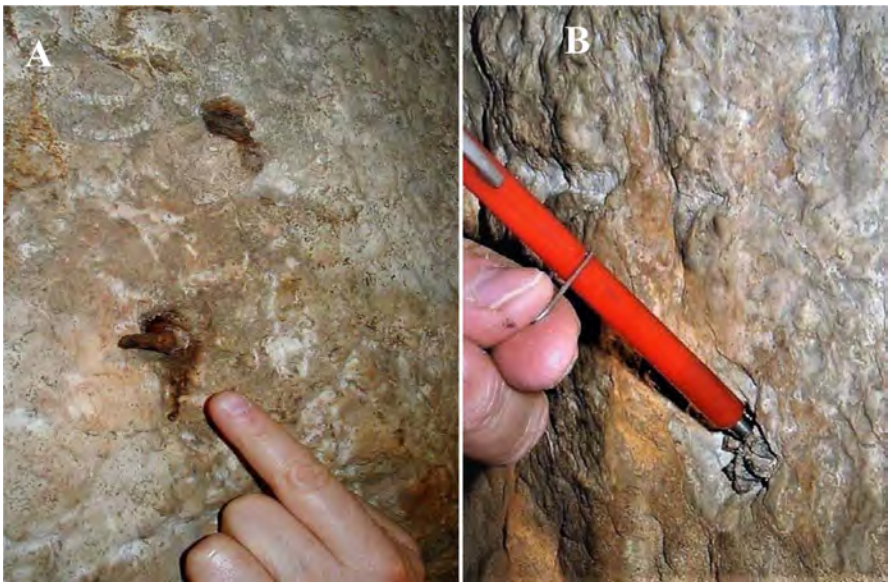

Figure 20. (A) NW wall). Two (of four) nails hammered into HT walls. One is shown (Nail 1) prior to complete removal from its position. (B) A red pen magnet attracted to Nail 2 (SE wall). The end of the nail appears to have been broken to give a rosette-shape of fractures. The head area is partially covered with a flowstone crust.

Figure 21. Two iron nails extricated from their source. Key: a-petrified wood, b- oxidized iron covering a metallic iron core, c-carbonate flowstone veneer with calcite, aragonite, gypsum and ankerite (Table 6, An. AS 6). The head area of Nail 1 (left edge) and bottom of Nail 2 (left edge) are both bent and the extremities are broken off. Indents in the nails made by hammering are not clearly visible in the photos.

iron wrought iron is relatively soft, ductile and has high elasticity and tensile strength. It has the advantage that it can be heated and reheated and worked (bent) into various shapes which have good corrosion resistance. The chemical composition of the metallic iron of the nails (Table 5, Table 6, An. 2, 24) their simple morphology and evidence of hammering indicates that they are wrought iron. The 1.39% and 2.6% carbon content of the nails is very low and compatible with wrought iron composition. These C concentrations may have been significantly magnified by the effects of the confining carbonate bed rock and calculation (normalization) of the EDS analyses to 100%.

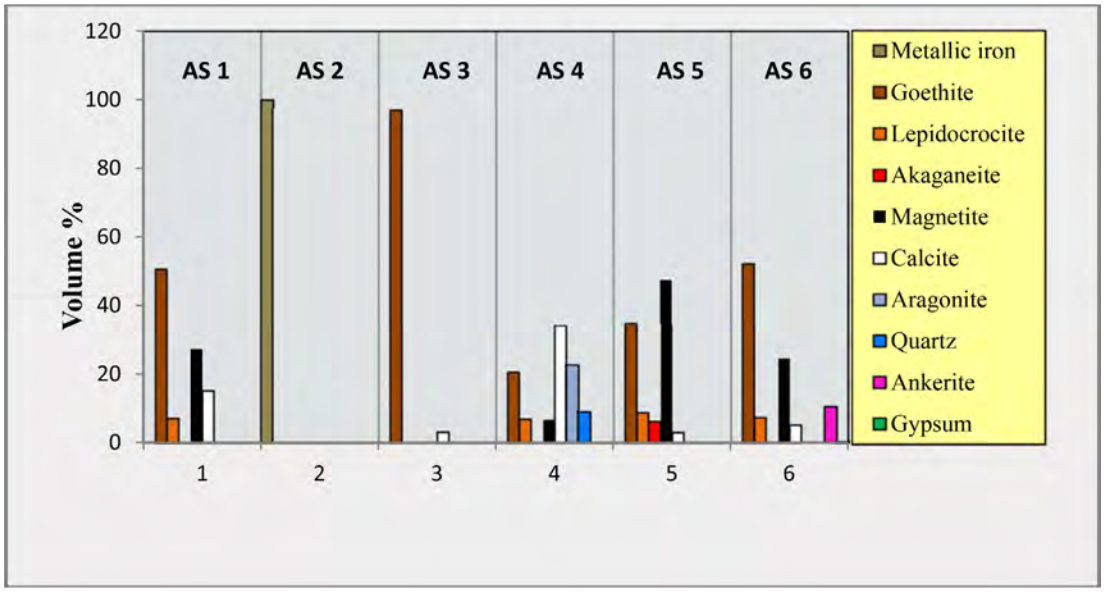

Figure 22. Columnar plot showing the types and volume % of iron oxidation products and trace mineral species which cover the head area (Nail 2) of the metallic iron core of the bolts.

Table 5. Semi-quantitative (SEM-EDS) chemical analyses of Hezekiah's Tunnel nails and proximate materials..

Sluice gate (spot) nails chemistry			Element (%)						
No.	Sample	Material	Si	Ca	Fe	Mg	Cl	C	O
1	A-01	Wood, fibers	1.38	1.91	52.87	0.87	-	15.37	27.61
2	A-03	Metallic iron	-	-	97.36	-	-	2.64	-
3	B-01	Wood, cell wall	0.78	5.85	70.64	0.33	0.68	10.90	10.83
4	C-01	Wood, fibers	0.49	1.00	62.36	0.69	-	9.90	25.56
5	D-01	Magnetite?	0.64	0.80	68.88	-	-	13.14	15.87
6	D-02	Wood, fibers	0.57	1.56	54.67	1.14	-	15.68	26.39
7	H2-006	Fe hydroxide	1.06	0.86	76.08		1.54	4.24	16.23
8	H2-015	Magnetite crystallites	-	-	85.01	-	-	-	14.99
9	H2-027	Akaganeite crystalites	-	-	77.44	-	4.46	-	18.10
10	H2-028	Akaganeite, rosette -like and fibrous crystallites	-	-	72.28	-	5.44	-	22.28

Continued

17	H3-002	Magnetite	-	-	73.52	-	-	-	26.48
18	H3-09	Mantled enclosures	-	-	81.01				14.99
19	H3-010	Mantled enclosures	-	-	76.52	-	-	-	23.40
20	H3-011	Skeletal crystals	-	-	60.41	1.09	-	4.23	34.28
21	H3-014	Bacteria cluster	-	-	78.69	-	-	-	21.31
22	Nail 1a	Lycoperdom fungi	0.98	11.09	38.26	0.94	0.83	13.75	34.15
24	Nail 2a	Metallic iron	-	-	80.83	-	-	1.39	17.78
25	Nail 2b	Akaganeite, coraline-like	-	-	68.33	-	4.79	2.44	24.44
26	Nail 2d	Magnetite cubes (?) beneath lamina of akaganeite	-	AL% 2.74 -	67.01	-	1.11	4.34	24.81
27	Patinated masonry	Biofilm enveloping bacteria cluster (pyrite precursor, Figure 27(B))	4.91	4.27	30.74	0.52	nd	12.44	-

Table 6. Mineral constituents (XRD) of the two oxidized iron nails from Hezekiah's Tunnel.

Minerals (%)	AS 1 Nail 1	AS 2 Nail 1	AS 3 Nail 1	AS 4 Nail 1	AS 5 Nail 2	AS 6 Nail 2	Environment of crystallization
Metallic Iron	0	100	0	0	0	0	Wrought iron, smelted from pyritic iron ore
Goethite α FeO(OH)	50.5	0	97	20.5	34.8	52.1	Crystalization at pH ~7 in moist – well oxygenated setting
Lepidocrocite γ FeO(OH)	7.1	0	0	6.8	8.7	7.3	Crystalization under anaerobic -hydromorphic conditions at pH~6
Magnetite Fe_3O_4	27.3	0	0	6.8	47.4	24.7	Biomineralization in basic, suboxic, anaerobic environment, pH > 7
Akaganeite (ß-FeOOH,Cl)	0	0	0	0	6.2	0	Hyper-chlorinated, acidic and oxidizing environment, pH < 7
Calcite $CaCO_3$	15.1	0	3	34.2	2.9	5.1	Flowstone deposit
Aragonite $CaCO_3$	0	0	0	22.7	0	0	Cave-type crystallization
Quartz SiO_2	0	0	0	9	0	0	Sandstone pockets in Gihon aquifer
Ankerite $Ca(Fe,Mg)(CO_3)_2$	0	0	0	0	0	10.6	Cave-type crystallization
Gypsum ($CaSO_4 \cdot 2H_2O$).	0	0	0	0	0	0.3	Cave-type crystallization

6.2. Wood Envelope: Iron Petrification, Microfabric and Biocolonization

It is quite amazing that both nails have retained, perhaps for a period of close to 3000 years, a partial envelope of well preserved although now fully petrified, wood (Figure 21, Figure 23(A)). Under the SEM, although most wood micro-structures are reasonably well preserved, the wood species is difficult to identify

with assurance as the wood slivers have suffered physical damage and chemical alteration. Prof. Werner H. Schoch (Labor fur Quartere Holtzer, Langnau Switzerland) examined the wood and was able to find a resin canal on a tangential fracture surface of a small wood fragment. The thick-walled epithelial cells and shape are typical of Cedrus sp. whereas Pinus sp. and Cupressaceae can be excluded with considerable certainty. Although we can argue that on the basis of the morphology of this resin channel that the wood is likely to be Cedrus the other anatomical features, such as the bordered pits in the rays are too poorly preserved for Cedrus to be confirmed with absolute confidence. Cedar did not grow in Iron Age Palestine, it was a rare and expensive import from Lebanon that, according to the Old Testament, was used in construction of the Temple in Jerusalem (circa 970 to 931 BCE).

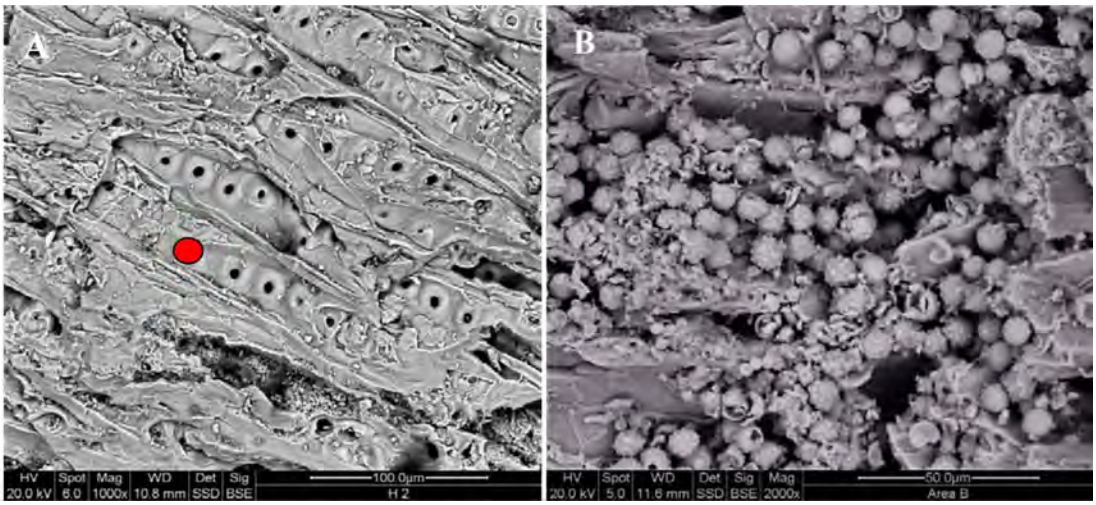

Figure 23. (A) Segment of wood accreted on Nail 2. Tracheids (wood cells with resin channel) show numerous pits in what is probably a tangential section of the cells. The small amounts of Si, Ca and Cl in the wood analyses is caused by contamination from incursions of tunnel moisture, the ~4% carbon concentration is probably all that remains from the original organic carbon. The high Fe content is due to slow replacement of wood carbon by goethite thereby recording one of a number of climate phases which affected the chemistry of the tunnel (see **Table 5**, An. 1-7). (B) Wood segment on Nail 1. The organic spheres that colonized the wood are probably spores of the fungus Lycoperdon (Puffball). Individual spheres are 6 - 7 um in size and exhibit projecting nano-globules~ 0.5 um in size.

The wood was colonized by spores which we have identified as Lycoperdon (puffball, **Figure 23(B)**). We emphasize that although the wood morphology was deformed during nail emplacement through wood panels followed by deterioration, the spores are perfectly well preserved. We reason that spore colonization of the wood slivers took place well after the nails were already hammered into HT walls. The wood and spores have been chemically altered to the iron hydroxide goethite (**Table 5**, An. A-01, B-01, C-01, D-02).

6.3. The Iron Oxidation Species (Fe-Oxides and Hydroxides): Goethite, Lepidocrocite, Akaganeite and Magnetite

Although physically confined to the microcosm of wall rock limestone enclosing

them our investigation has provided us with an unexpected wealth of information derived from an extraordinary range of secondary Fe-oxide and hydroxide mineral species identified. The latter include the minerals goethite [α-FeO(OH)], lepidocrocite [γ-FeO(OH)], biomagnetite (Fe_3O_4) and akaganeite [$Fe^{3+}O(OH,Cl)$], (**Figure 22**, **Table 5**, **Table 6**)]. Goethite is a common pigment in ocher and lepidocrocite is most commonly encountered as rust on the interior of steel pipes. The chloridic iron hydroxide akaganeite achieved fame because it is best known from its presence in "extraterrestrial materials" including a Martian meteorite, in samples collected from the moon's surface by the crew of Apollo11 and notably it was also detected on Mars by orbital imaging spectroscopy (Carter et al., 2015). Collectively these species provide important testimony to what we view as an extensive period of fluctuating physical and chemical conditions within the immediate environment of the nails but undoubtedly also within the aqueduct as a whole.

Goethite would be the preferred Fe-hydroxide to crystallize during initial oxidation of the metallic iron while the aqueduct was being initiated and fresh spring waters were surging through the clean tunnel. Such conditions would result in good oxygenation and an elevated pH of the water system. We reason that better flow conditions prevailed in the tunnel during its early stages, that is during the early years after tunnel opening. On the other hand, slow water transport and high concentration of sediment would in time result in periodic blockages in the tunnel and long periods of standing brackish water culminating in anaerobic physico-chemical conditions. Such a chemical milieu would favour the crystallization of lepidocrocite—the less stable, infrequently encountered polymorph of goethite (Ross & Wang, 1982, Schwertmann & Taylor, 1972). Lepidocrocite crystallizes preferably when iron oxidizes under hydromorphic conditions in an anaerobic environment dominated by standing water such as characterizes marshes and bogs. Such a chemical setting is acidic with pH values below 7. The high quartz content of the spring waters, and therefore the tunnel sediment (**Figure 6(B)**) would contribute to a drop of pH, conditions that would favour the crystallization of lepidocrocite rather the goethite. The most recent 7.1 pH value for the spring (Amiel et al., 2010) is rather low for such a limestone terrain where pH values would, under normal circumstances, be similar to that of groundwater flowing through limestone strata where values can be as high as 8.5. We reason that 19th and 20th century urban contamination must have significantly increased the pH and thus alkalinity level of the spring.

7. Biomineralization: The Crystallization of Biomagnetite

7.1. Background

A change, more profound than crystallization of the two iron hydroxide species discussed above, took place during the latter part of the long history of the rusting nails. It is evidenced by the crystallization of two unusual secondary iron species - magnetite (Fe_3O_4) and akaganeite (ß-FeOOH, Cl (**Figure 24**, **Figure 25**).

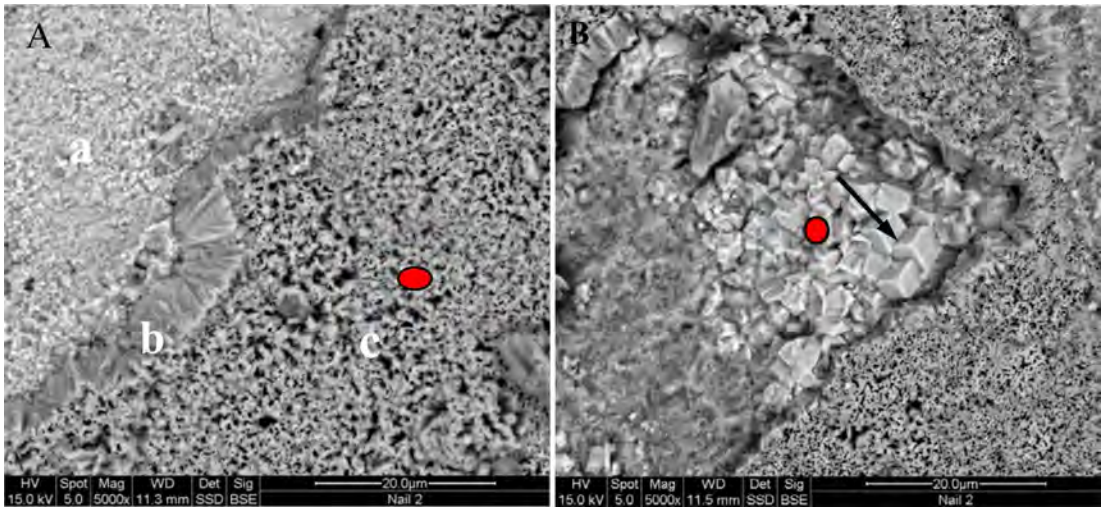

Figure 24. (A) Goethite (a), scaly sheaf-like lepidocrocite (b) and coraline-like akaganeite (c) (Table 5, An. 25). (B) Magnetite crystallites substratum (a) beneath a fine (~10 μm thick) fibrous crust of akaganeite. The presence of Cl is contamination from neighboring akaganeite. We attribute the moderate C concentration to traces of organic carbon remaining from the original bacterial source. Chemical analysis (Table 5, An. 26 red marker) is on magnetite beneath a veneer of akaganeite. The dominant crystal forms (at arrow) appear to be cubic and/or cuboid (rectangular shaped).

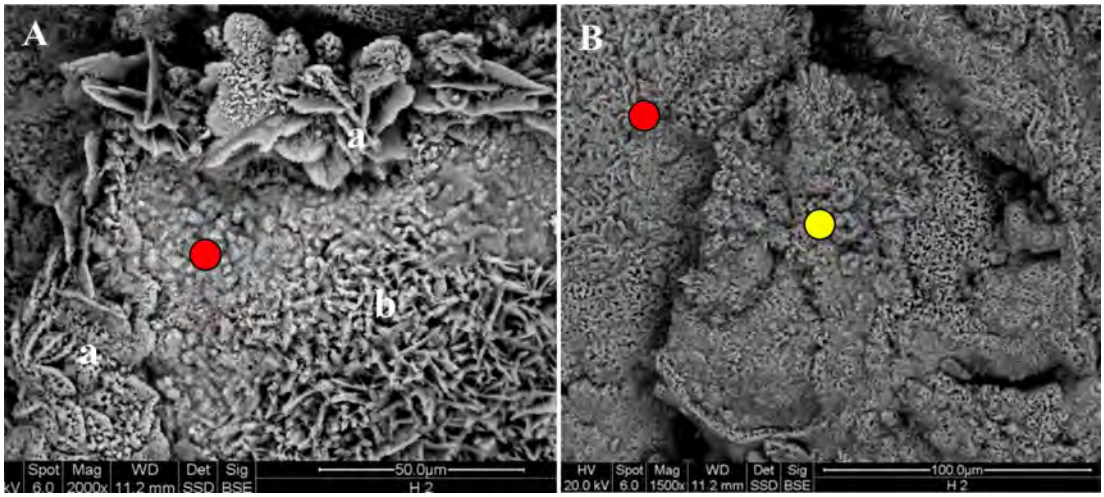

Figure 25. (A) Sheaf-like scaly lepidocrocite (a) and rod-like (tubular) fibrous akaganeite (b). (B) Coraline akaganeite, confirmed by the presence of 5.44% Cl and XRD analyses (Analyses, Table 5, H2-027 on red marker and H2-028 on yellow).

Magnetite nucleated by means of biomineralization within a kind of magnetosome-like membrane-covered enclosure. A later, no less significant change within the microcosm of the nails is marked by the appearance of the rare chloridic Fe-hydroxide akaganeite. Magnetite was identified in most samples scrapped from the surface crust of the two nails, after goethite it is the dominant iron oxide and constitutes up to 50% of some samples, with smaller concentrations of lepidocrocite and considerably less akaganeite present (Figure 22). An exceptional case of idiomorphic crystals with a cubic and/or cuboid form and close to magnetite in chemical composition can occasionally be seen buried beneath a lamina

of spindly and coraline-like mass of akaganeite (**Table 5**, An. 26, **Figure 24(B)**). With the exception of slivers of petrified wood and late deposits of carbonate flowstone, gypsum and ankerite most of the hard, black surface layer on the nails is magnetite. Magnetite is known to be a non-corrosive species and consequently may have protected the metallic iron in the interior of the bolts from rusting.

The term biomineralization refers to transformations of certain types of organic substances to a diverse group of inorganic derivatives by living micro-organisms. Bazylinski (Bazylinski, 1996; Bazylinski et al., 2007) grouped such bio-processes into two modes 1) biologically induced mineralization (BIM) and 2) biologically controlled mineralization (BCM). In BCM, for example, microbes apply a great degree of chemical and genetic control over the nucleation and growth of mineral particles because the biominerals produced serve some physiological function. One group of such micro-organisms, the magnetotactic bacteria (MTB) which we here focus on, are a "diverse assemblage of mainly aquatic bacteria. They are able to align and swim along geomagnetic field lines, an important phenomenon referred to as magnetotaxis (ref. above and Blakemore, 1975). Magnetotaxis results from the presence of magnetosomes–kinds of membranes which enclose nano-size magnetite crystals which are arranged in a chain-like alignment (**Figure 26**). Individual crystals are slightly elongated in the direction of the chain with dimensions in the range of 35 to 120 nm (0.035 - 0.12 μm) but may also reach lengths of 200 - 250 nm. Another group of bacteria may form magnetite intracellularly, these nucleate within preformed vesicular structures (ref. above). Biomagnetites for example, can be produced by both modes within magnetosomes but also in preformed vesicles in the same sedimentary environment.

The preferred chemical environment for magnetite formed by bacterial activity is within the basic and reducing suboxic (oxic-anoxic) transition zone at a pH close to neutral or slightly > 7. In this environment biologically-induced mineralization will take place if the metabolic activity of microbes produced chemical conditions favorable for mineral formation (e. g. Faivre & Zuddas, 2006). The iron used by bacteria in the formation of MTB magnetosomes can be derived from available Fe^{+2} or Fe^{+3} in the immediate environment, or as we show here - from rusting nails directly supplied to bacteria that absorbed iron as they colonized the nails. Based on data above we emphasize the unique chemical constraints, within the milieu of the rusting iron nails, for biomineralization to activate the crystallization of biomagnetite on the one hand, and chloridic akaganeite (below) on the other.

Magnetosomes and Invagination: Zucker et al. (2016) divided the generation of magnetosomes into several steps they include: 1) vesicle formation and invagination 2), the transfer of iron into vesicles 3) biomineralization and 4) the alignment of magnetosomes into oriented chains. Invagination, an important step in the process of biomineralization, is defined as "the mechanism that takes place during gastrulation" (gastrulation occurs when a blastula made up of one layer, folds inward and enlarges to create a gastrula which has three germ layers (Mechanism of Invagination. png (923×558) (wikimedia.org). What we argue

below (Figures 26-29) we view as a similar evolutionary process from the coalescence of iron bacteria to vesicle formation (mantled enclosures) followed by infolding of the membranes (invagination). The process culminates with magnetite crystals emerging from the enclosures with some showing a tendency to coalesce into growing chains (Figure 30). Friedmann et al. (2001) argued that the formation of magnetite crystals within a definite size range and their arrangement in linear chains is "in itself a conspicuous example of genetically controlled biomineralization", and furthermore "no inorganic process is known to produce similar structures". We emphasize that the magnetite chains seen in the magnetites on the HT nails exhibit most of the attributes for biomineralization processes as listed by Friedmann et al. (2001) above.

7.2. Biomagnetite on the Nails: Fe-Bacteria, Biofilms, Mantled Enclosures and Magnetite in Chains

Within the Fe-oxidized zone of the HT nails we have found spheroids dispersed or coalesced in clusters of globules we interpret as bacteria cocci (Figure 28, Figure 29). Chemically the globules and all the proximal morphologies are composed entirely of FeO with a composition identical or close to that of magnetite (Table 5, An. H3-09, H3-010, H3-011, H3-014). The globules occur 1) as dispersed spheres, in 2) cone-shaped clusters and 3) seen with some difficulty within a type of membrane which, for lack of better term, we refer to as a mantled enclosure (ME) within which 4) they seem to at first crystalize as incipient-skeletal precursors of fully crystalline magnetite (Figure 28, Figure 29). At some point in this evolutionary process the membrane enclosing the nano-globules seems to perforate or fold inwards (Figure 28)—a process we interpret as a kind of invagination that we discussed above. This evolutionary sequence culminates with 5) the emergence of poorly shaped magnetite crystallites

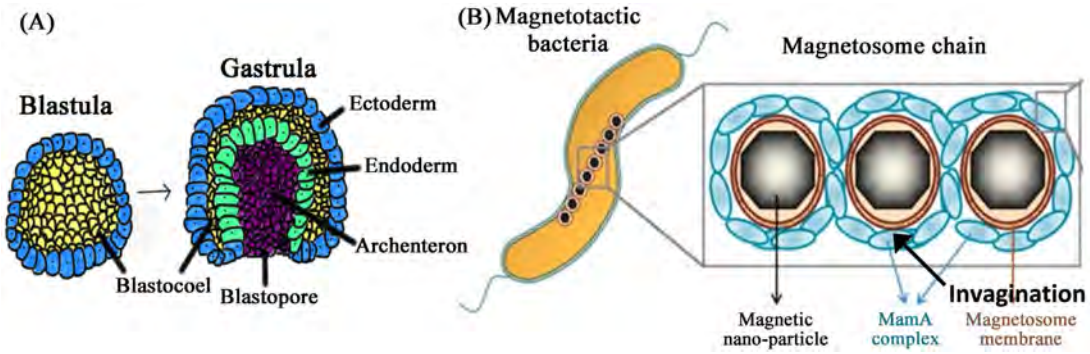

Sources: (A): Invagination: https://doi.org/10.3390/pharmaceutics13081262. (B) Gastrulation: https://en.wikipedia.org>wiki>Gastrulation.

Figure 26. The figures show typical morphological features and the evolutionary process of nucleation and evolution of specific types of magnetotactic bacteria. The processes involves invagination and gastrulation, both take place when a blastula composed of one layer, folds inward and enlarges to create a gastrula (above) which is composed of three germ layers. The process involves the conversion of an embryo from a simple spherical ball of cells into a complex multi-layered organism. Gastrula is a multicellular embryo, it develops from a blastula-a hollow single-layered ball of cells.

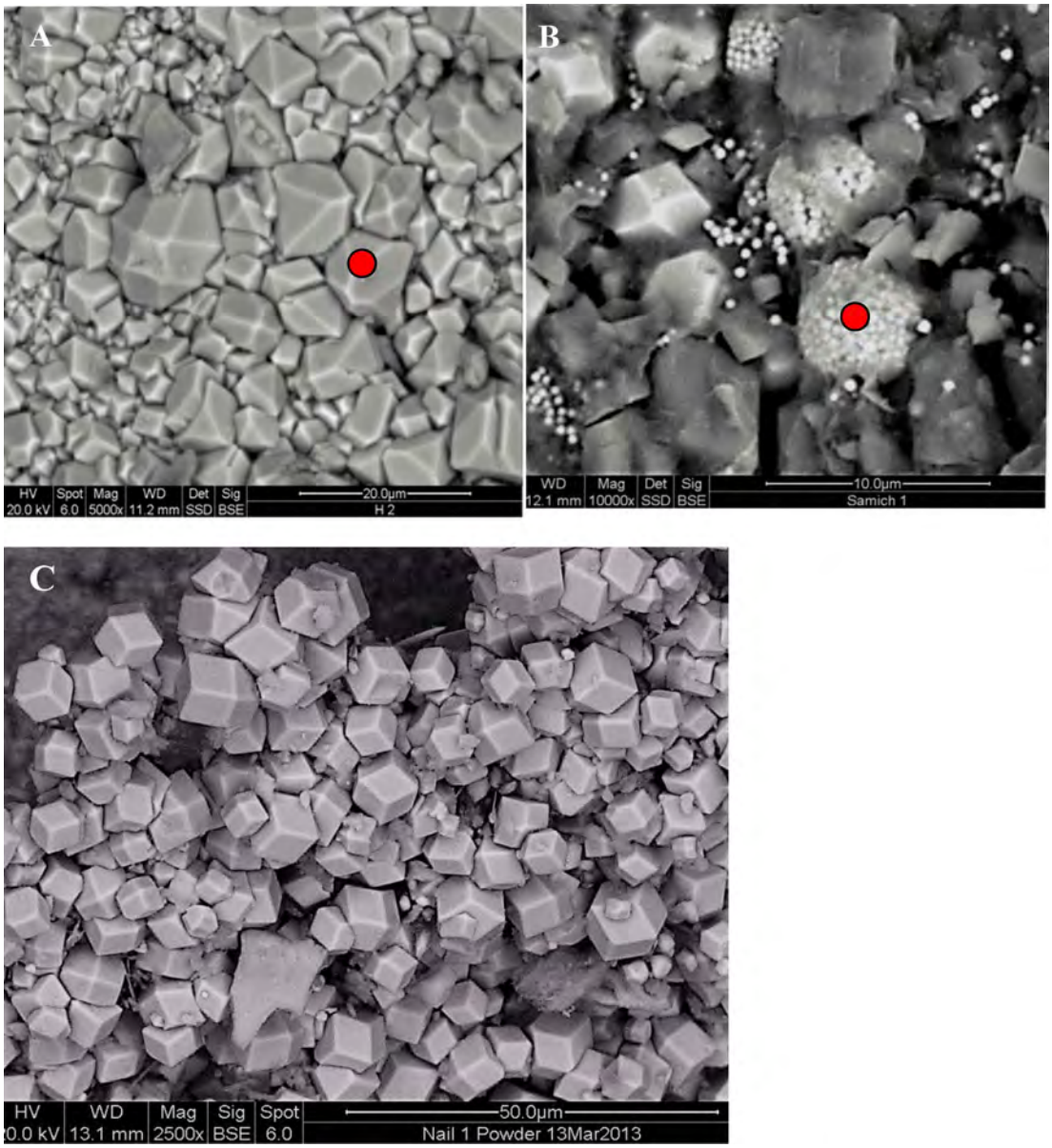

Figure 27. (A) Field of magnetite crystals, in our interpretation they exhibit the final stage of the conversion of Fe-bacteria to magnetite crystals here emerged from mantled enclosures as shown in **Figure 28** and **Figure 29**. The magnetite crystal forms are truncated octahedra and some dodecahedra. **Table 5**, An. H2-015). (B) An example of biomineralization of pyrite. Clusters of bacteria are enclosed by biofilms out of which emerge idiomorphic pyrites. Some grown pyrite is seen to be still enclosed by a a kind of membrane. The bacteria are ~0.4 um in size, the biofilm enclosures are ~5 - 7 µm in size (**Table 5**, An. 27). Sample derived from construction masonry surface patinated by urban pollution. (C). Caiaphas tomb. Biomagnetites in the crust of oxidized Nail 2 (Shimron et al. 2020). Crystal forms include, dodecahedra, cubes and cuboids. Some crystals are twinned.

or in well shaped idiomorphic magnetite (**Figure 30**). In order to clarify the above process of crystallization of biomagnetite in mantled enclosures we compare these structures with the nucleation of crystaline pyrite within cocoon-like biofilms packed with FeS-rich bacteria. The latter can be seen on miscolored limestone masonry surfaces contaminated by urban pollution (Shimron unpublished data and (**Figure 27(B)**). The biomagnetites (**Figure 27(A)**, **Figure 30**)

exhibit a broad range of sizes, from less then 1 μm to greater then 10 μm in size and up to four crystal forms, cubes, cuboids, pyramids and dodecahedra (Figure 27(A), Figure 27(B)). Where arranged or coalesced into chains individual crystal sizes in a chain range from ~1.0 - ~6 μm with each chain connecting crystallites of a single specific size. It appears that magnetite growth and coalescence into chains progressed contemporaneously. The chains do not exhibit any evidence of what may constitute fossil MTB morphologies.

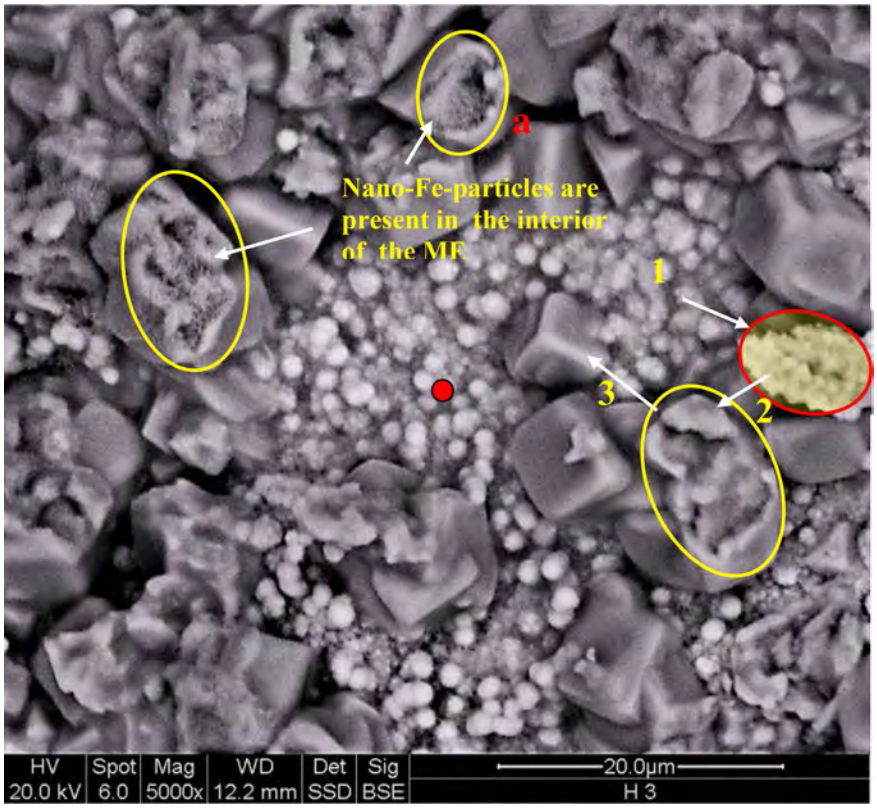

Figure 28. The figure above shows the close genetic link between globules (Fe-bacteria) and, for lack of a better term, what we refer to as mantled enclosures (ME). Some of the latter structures, many of which are perforated, appear to have a cubic crystalline morphology. The interior of the ME seem to be filled with nano-particles (e.g. at a) a feature we interpret as a kind of "invagination" (Ref: https://en.wikipedia.org/wiki/Invagination). We reason that the nano-particles are predecesors of magnetite crystallites, part of an evolutionary process (1 - 3 above) that will culminate in a field of magnetite crystals (Figure 30). The globules are ~1.0 μm and the mantled structures are ~5 - 6 μm in diameter. Although we sought, we have not found identical mantle-enclosed structures anywhere in published scientific literature (Chem. analyses Table 2, Table 3, Table 5).

8. Akaganeite

We have shown examples of akaganeite identified on the HT nails in the presence of goethite, lepidocrocite and magnetite (Figure 24, Figure 25), Akaganeite occurs in micro-laminae of spindly fibrous crystalites or in coraline-like crusts overlying crystalline magnetite. The chemical setting in the immediate microcosm of the nails during crystallization of biomagnetite was anaerobic, reducing

and suboxic at a neutral or slightly elevated (>7) pH. These well constrained chemical conditions underwent a considerable change as the Gihon Spring waters became hyper-chlorinated, acidic and oxidizing. Such a switch in the chemistry of the Gihon and other water sources in the area may have been imposed throughout the region with the widespread chloridization of water during the later part of the 1970's. Apparently in consequence of regional chloridization of water sources we identified on Nail 2, by XRD and subsequently confirmed with SEM-EDS analyses the presence of small amounts of the iron chloride hydroxide akaganeite (ß-goethite - FeOOHCl). The mineral is known to be rare in natural settings as it requires unique chemical conditions in its environment for nucleation and growth. The chemical prerequisites for akaganeite crystallization are high salinity, mild acidity (pH~6), oxidizing conditions, and most important a high concentrations of iron (II/III) and chlorine (Font et al., 2017; Remazeilles & Refait, 2007). First identified in a Japanese mine, akaganeite is mainly known from the Deccan Trap volcanic province in India but was also found in areas of hot brines and in iron rust on steel in marine environments (e.g., Morcillo et al., 2015). It is well known from reports of its identification, by orbital imaging

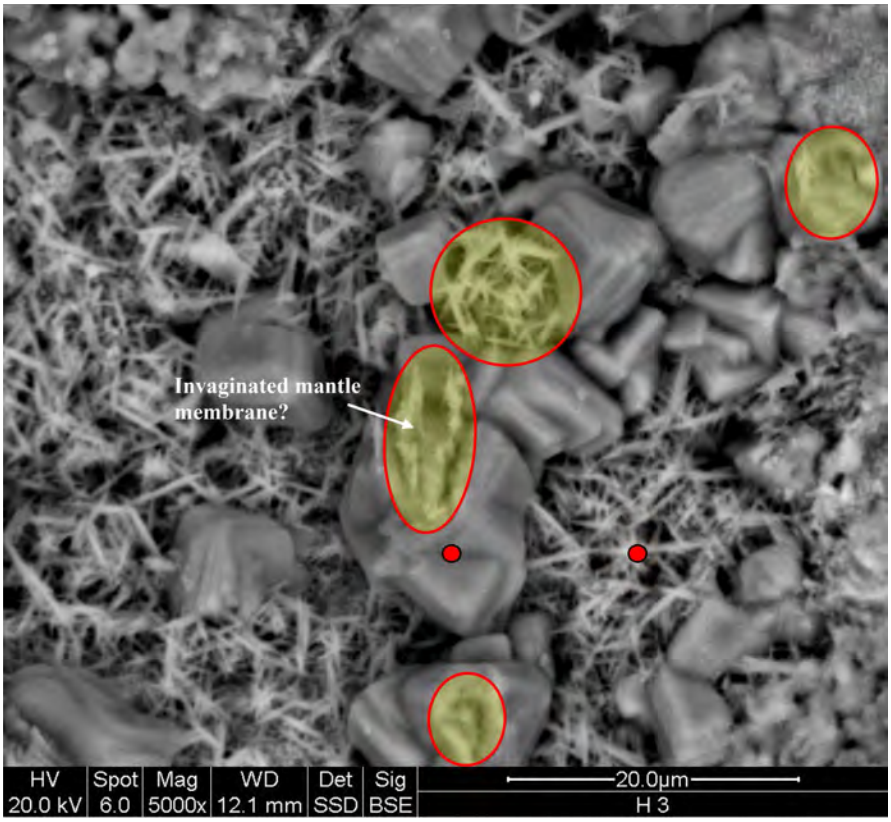

Figure 29. The figure shows what may be a more advanced stage of mantled enclosure evolution with nano-particles (**Figure 28**) now evolved into skeletal crystallites with magnetite composition. We question if the next - final stage, in this evolving process would culminate in a field of magnetite crystals some of which here "coalesced" into chains of crystals of specific size (**Figure 30** and see **Table 5**, An. H2-015, H3-09, H3-010, H3-011, H3-014).

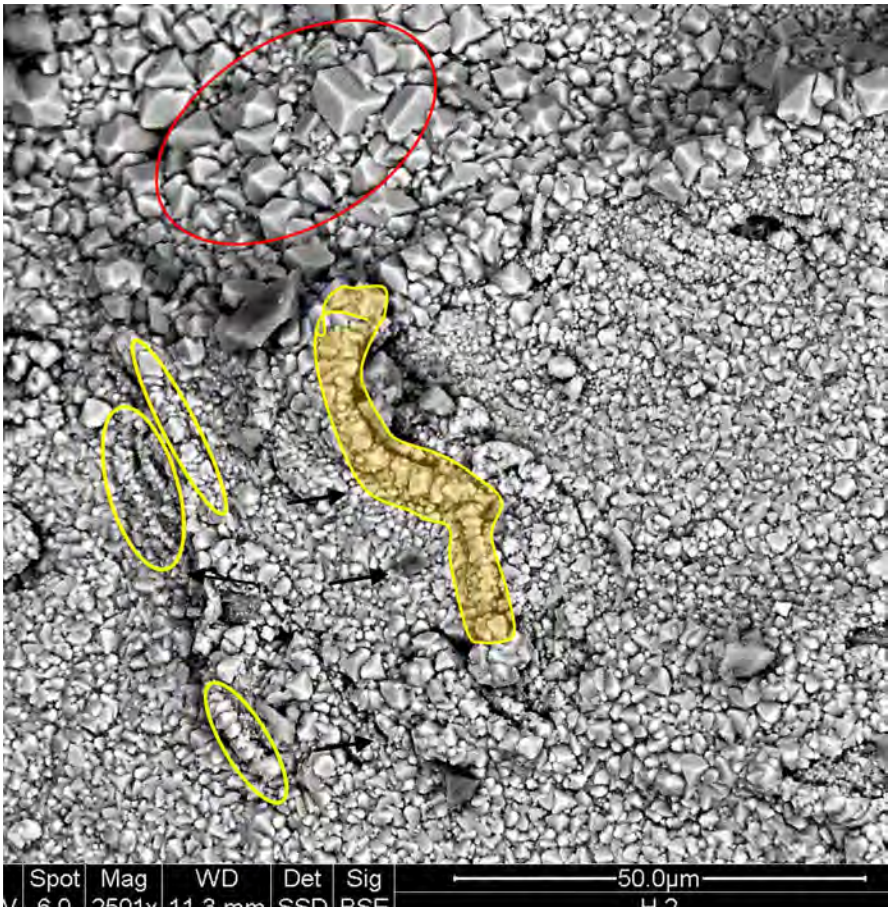

Figure 30. A complex field of magnetite crystals, the crystals range from ~1 µm to ~10 µm in size with some of a specific size drawn into chain-like, occasionally curving, structures. There is a distinct change in the crystal quality and size of magnetite crystals between the upper part of the magnetite field and the lower segment with the chains. Individual crystal sizes in the chains range from ~0.5 µm and up to 3 µm in size. Individual chains are 10 - 20 µm some reaching up 80 µm in length. The increase in size of crystals from chain to chain suggests crystal growth continued while, or after the chains had already formed. Compare magnetite chains above and bacteria clusters (**Figure 28**) with those in Martian meteorite ALH84001 (Thomas-Keprta et al., 2009). Encircled red are octahedral and cuboid crystal forms.

spectroscopy, at several locations on Mars, in rocks brought from the moon during the Apollo Project and its presence in some meteorites (Carter et al., 2015; Font et al., 2017). Carter suggested that the identification of akaganeite in at least three basins on Mars implies the existence of near-marine (lagoon-like) evaporitic settings already early in Martian history.

9. Discussion

Near the beginning of the 8th century BCE as the armies of Sennacherib, king of Assyria and ruler of Nineveh (705 - 681 BCE) were approaching Palestine political unrest dominated the southwestern Middle East. Israelite king Hezekiah, motivated by severe security issues was compelled to protect Jerusalem's only

natural water source by modifying the preexisting Gihon Spring waterworks. Hezekiah's engineers were well aware that excavating and diverting water from the Gihon Spring area south into the Siloam pool would lower the water level in the main northern heart of the city thereby forcing it to rely on the erratic activity of a pulsating spring while leaving the three main water reservoirs periodically high and dry. Already at this time Hezekiah's engineers must have concluded that construction of a well sheltered and movable damming source with the capability of lowering and raising water level in the aqueduct was crucial and required execution while the tunnel was still dry. We sought and found powerful evidence for just such a device at the only location where it could function, protected yet flexible to changing security circumstances. The device, if proven to date to Iron Age II, is—to the best of our knowledge, the oldest sluice gate known and now recorded. As historical records show Sennacherib besieged but did not conquer Jerusualem. This formidable task was more capably executed two decades later in 721 BCE when the Assyrian king Sargon II dispersed the twelve tribes of Israel and conquered Palestine. The rest is history.

The Sluice Gate and the Stained Ceiling Zones 1 - 3: Material evidence for the existence of a sluice gate in Hezekiah's aqueduct includes four rusted, apparently very ancient, bolts enveloped by petrified wood, found hammered into opposite walls of the aqueduct. Subsequent related finds include the recognition of anthropogenic modifications to the tunnel ceiling above the walls carrying the bolts. These efforts include applications of three compositionally different plaster layers covering three pronounced ceiling fracture zones. Two of the plaster applications (Zones 2 and 3) carry (arguably) bottom ash spheroids and high temperature slag and other base metal-bearing components possibly derived from iron ore. They include pyrite, ilmenite, and unknown ZnCu and FeCa mineral phases. Since a similar variety of black, slaggy mortar from a blocking wall in the northern segment of the Gihon waterworks was dated to the Mamluke period, the workings in fracture Zone 2 and Zone 3 can be viewed as repairs and/or modifications to the sluice and area carried out by Mamluke rulers. Black, organic carbon-rich grains present in Zone 1 plaster and also embedded in calcified fibers, are chemically compatible with soot (Gupta et al., 2019) here probably contributed from oil lamps or torches used by sluice gate workers. We attribute the planar, apparently polished, faces of calcified organic fibers to abrasive action between two objects - one moving and one stationary. Collectively they point to extensive anthropogenic activity linked to the sluice gate construction and usage.

Mamluke slaves, turned generals, ruled Palestine 1260 - 1516 AD. Locally they are known in particular not only for their military prowess but also for their well preserved architectural edifices, including madrasas, markets, public baths and fountains. Their artistic flair was however focused on the decorative arts including glass, woodwork and inlaid metalwork in particular. Window gratings of metallic iron still decorate many magnificent Mamluke edifices in Jerusalem un-

til the present. Based on our finds of slag and high temperature gangue minerals in mortar from a blocking wall near the Gihon Spring and now also above the sluice implies that a Mamluke Period iron smelting plant, probably using imported iron ore was functioning in Jerusalem of that period. One potential source of metal ores since antiquity in the Eastern Mediterranean region is the Laurion area near Athens, Greece.

The secondary iron oxidation products on the nails: their significance with respcct to the changing geochemical setting in the aqueduct. It is amazing that within an area of a few square cms of rust we have identified three Fe-hydroxide and one Fe-oxide (magnetite) species the last of which we are able to link with bacterial activity. Akaganeite, the last Fe-oxidation product to crystallize on the nails, is a rare chloridic iron hydroxide, although known from the Deccan Traps volcanic province and as a corrosion product of steel, it is especially known for its presence in Martian materials. We can conclude, with considerable confidence, that the chemical setting in the tunnel must have changed in time from 1) a moist and well oxygenated setting (goethite) to 2) hydromorphic anaerobic conditions (lepidocrocite) to 3) physico-chemical conditions during which colonization by a bacterial species which initiated biocrystallization (magnetite) under what were basic, suboxic-anaerobic conditions. Finally, with passing time the chemical setting in the tunnel changed again culminating in 4) a hyper-chlorinated, acidic and oxidizing setting which favored crystallization of akaganeite. Such fluctuating chemical conditions required a long time span for the different mineral species to nucleate, mature and reach fruition. Some of the more pronounced chemical changes in the tunnel may have resulted when water from different sources arrived into the city, this especially following completion of the Hellenistic (1 - 2nd century BCE) and later the Roman period (1st century CE) aqueducts. Additional significant changes in the chemistry of the water sources also took place during the population explosions in the city during the Byzantine (3rd to 6th century CE) and Islamic periods (6th to 15th century CE) and finally in the 1970's with the addition of chlorine into water sources throughout the region.

10. Conclusion

Near the end of the 7th and beginning of the 8th century BCE the leadership of Hezekaiah's kingdom faced two potentially serious threats, the first in the form of the approaching armies of the Assyrian ruler Sennacherib, the other a potential acute shortage of water in the Gihon spring reservoirs which provided water to the heart of the rapidly growing city following its early 8th century BCE urban revival. To deal with the second issue engineers of the newly constructed aqueduct realized that a movable, well protected dam-like installation which could control the level of water in the tunnel was an imperative. This was carried out and a sluice gate was constructed in the newly completed aqueduct. Four parameters provide the basis in our view that the sluice was activated already during, or soon following inauguration of the aqueduct in the 8th century BCE, they are:

1) the Assyrian threat to Jerusalem's water supply was acute and immediate; 2) in order to secure the water supply to the city's religious and cultural core, control of water level in the aqueduct, and thereby in the Gihon Spring water reservoirs was of essence; 3) water level (sediment laminae) markers in the aqueduct indicate that at least some wall sediment deposits predate deposition of cave flowstone the oldest which we dated to the 4th century BCE and finally 4) the four iron oxidation products of the sluice gate bolts point to a long history of, sometimes dramatically, changing chemical and micro-climate conditions in the tunnel. We hypothesise that structural problems in the morphology of the sluice gate setting (the NW wall) are a much younger, Mamluke Period, or younger, modification of the sluice gate infrastructure. We can only speculate what the objectives of the later were, consequently at this time they remain a mystery.

Acknowledgments

We wish to thank, in particular, Dr. Naama Sukenik, Curator of Organic Materials at the Israel Antiquities Authority and Prof. Margarite Gleba of the University of Padua who contributed to this manuscript by examining and commenting on the SEM images of organic-fiber like materials from alteration Zone 1 above the sluice gate. We are most grateful to Dr. Ludwik Halitz from the Israel Geological Survey (ret.) for much advice but especially for taking time to discuss the chemical data with the senior author. Prof. Anthony Phillpots of the University of Connecticut, Storrs USA, contributed significantly to the manuscript with numerous corrections and criticisms where such were justified. Our (AES) thanks to Dr. Thomas-Keprta of NASA for taking time to discuss some possible similarities, and dissimilarities, between biomineralization on Martian meteorite ALH84001 and that on HT nails. Our deep gratitude to the referees of the submitted manuscript, their constructive comments are incorporated within the present version of the manuscript. Dr. Moshe Shirav and technician Shelomo Askenazy, both colleagues from the Israel Geological Survey (ret.) have assisted in the sampling program and discussions in particular pertaining Zones 1 - 3. Their field assistance and contributory comments are much appreciated. My (AES) deep thanks to friend Prof. Alan Rosenthal and my daughter Liat Shimron both of whom struggled with my English and made the manuscript more readable.

Conflicts of Interest

The authors declare no conflicts of interest regarding the publication of this paper.

References

Amiel, B. R., Grodek, T., & Frumkin, A. (2010). Characterization of the Hydrogeology of the Sacred Gihon Spring, Jeerualem: A Deteriorating Urban Karst Spring. *Hydrogeology Journal, 18,* 1465-1479. https://doi.org/10.1007/s10040-010-0600-6

Amiram, R. (1976). The Water Supply of Israelite Jerusalem. In Y. Yadin (Ed.), *Jerusalem Revealed, Archaeology in the Holy City 1968-1974* (pp. 75-78). Yael University Press

and the Israel Exloration Society.

Bazylinski, D. (1996). Controlled Biomineralization of Magnetic Minerals by Magnetotactic Bacteria. *Chemical Geology, 132,* 191-198. https://doi.org/10.1016/S0009-2541(96)00055-1

Bazylinski, D. A., Richard, B., Frankel, R. B., Kurt, O., Konhauser, K. O. (2007). Modes of Biomineralization of Magnetite by Microbes. *Geomicrobiology Journal, 24,* 465-475. https://doi.org/10.1080/01490450701572259

Blakemore, R. P. (1975). Magnetotactic Bacteria. *Science, 190,* 377-379. https://doi.org/10.1126/science.170679

Carter, J., Viviano-Beck, C., Loizeau, D., Bishop, J., & Le Deit, L. (2015). Orbital Detection and Implications of Akaganeite on Mars. *Icarus, 253,* 296-310. https://doi.org/10.1016/j.icarus.2015.01.020

Faivre, D., & Zuddas, P. P. (2006). An Integrated Approach for Determining the Origin of Magnetite Nanoparticles. *Earth and Planetary Science Letters, 243,* 53-60. https://doi.org/10.1016/j.epsl.2006.01.012

Font, E., Carlut, J., Rémazeilles, C., Mather, T. A., Nédélec, A., & Casale, J. M. (2017). End-Cretaceous Akaganéite as a Mineral Marker of Deccan Volcanism in the Sedimentary Record. *Scientific Reports, 7,* Article No. 11453. https://doi.org/10.1038/s41598-017-11954-y

Friedmann, E. I., Wierzchos, J., Ascaso, C., & Winklhofer, M. (2001). Chains of Magnetite Crystals in the Meteorite ALH84001: Evidence of Biological Origin. *Proceedings of the National Academy of Sciences of the United States of America, 98,* 2176-2181. https://doi.org/10.1073/pnas.051514698

Frumkin, A., & Shimron, A. (2006). Tunnel Engineering in the Iron Age: Geoarchaeology of the Siloam Tunnel, Jerusalem. *Journal of Archaeological Science, 33,* 227-237. https://doi.org/10.1016/j.jas.2005.07.018

Frumkin, A., Shimron, A., & Rosenbaum, J. (2003). Radiometric Dating of the Siloam Tunnel, Jerusalem. *Nature, 425,* 169-171. https://doi.org/10.1038/nature01875

Gill, D. (1991). Subterranean Waterworks of Biblical Jerusalem: Adapatation of a Karst System. *Science, 254,* 1467-1470. https://doi.org/10.1126/science.254.5037.1467

Gill, D. (1994). How They Met. *Biblical Archaeology Review, 20,* 21-23.

Gill, D. (2012). *The MB II Warren Shaft Water Well in the City of David, Jerusalem.* Geological Survey of Israel Report No. 55 (569.4).

Gupta, P., Jangid, A., & Kumar, R. (2019). Chemistry of Carbon Soot Particles and the Role of Neighboring Components. In *Proceedings of Fall Meeting 2019 of American Geophysical Union*. American Geophysical Union.

Meron, E. (2002). A New Look at Jerusalem's Water System during the Middle Bronze ll Period. In C. Ohlig, Y. Peleg, & T. T. Siegburg (Eds.), *Proceedings of the 11th International Conference on the History of Water Management and Hydraulic Engineering in the Mediterranean Region, Israel* (pp. 7-13). Cura Aquarum in Israel.

Morcillo, M., González-Calbet, J. M., Jiménez, J. A., Díaz, I., Alcántara, J., Chico, B. et al. (2015). Environmental Conditions for Akaganeite Formation in Marine Atmosphere Mild Steel Corrosion Products and Its Characterization. *COROSSION, 71,* 872-886. https://doi.org/10.5006/1672

Norin, S. (1998). The Age of the Siloam Inscription and Hezekiah's Tunnel. *Vetus Testamentum, 48,* 37-48. https://doi.org/10.1163/1568533982722063 https://www.jstar.org/stable/1585460

Pense, A. W. (2000). Iron through the Ages. *Materials Characterization, 45,* 353-363.

https://doi.org/10.1016/S1044-5803(00)00105-4

Reich, R., & Shukrun, E. (1999). Light at the End of the Tunnel. Warren's Shaft theory of David's Conquest Shattered. *Biblical Archaeology Review, 25,* 22-23+72.

Reich, R., & Shukrun, E. (2000). The Excavations at the Gihon Spring and Warren's Shaft System in the City of David. In H. Geva (Ed.), *Ancient Jerusalem Revealed* (pp. 327-329). Israel Exploration Society, Jerusalem.

Reich, R., & Shukrun, E. (2003). Jerusalem, City of David. *Hadashot Arkheologiyot, Excavations and Surveys, 114,* 77-78.

Reich, R., & Shukrun, E. (2004). The History of the Gihon Spring in Jerusalem. *Levant, 36,* 211-223. https://doi.org/10.1179/lev.2004.36.1.211

Reich, R., Avni, G., & Winter, T. (1999). *The Jerusalem Archaeological Park* (165 p). Israel Antiquities Authority.

Remazeilles, C., & Refait, Ph. (2007). On the Formation of ß-FeOOH (Akaganeite) in Chloride Containing Environments. *Corosion Science, 49,* 844-857. https://doi.org/10.1016/j.corsci.2006.06.003

Rogerson, J., & Davis, P. R. (1996). Was the Siloam Tunnel Built by Hezekia? *Biblical Archaeologist, 59,* 138-149. https://doi.org/10.2307/3210545

Ross, J. G., & Wang, C. (1982). Lepidocrocite in a Calcareous, Well-Drained Soil. *Clays and Clay Minerals, 30,* 394-396. https://doi.org/10.1346/CCMN.1982.0300511

Schwertmann, U. & Taylor, R.M. (1972). The Transformation of Lepidocrocite to goethite. *Clays and Clay Minerals, 20,* 151-158. https://doi.org/10.1346/CCMN.1972.0200306

Sebela, S., Miler, M., Skobe, S., Torkar, S., & Zupancic, N. (2015). Characterization of Black Deposits in karstic Caves, Examples from Slovenia. *Facies, 61,* Article No. 6. https://doi.org/10.1007/s10347-015-0430-z

Shiloh, Y. (1981). Jerusalem's Water Supply during Siege—The Rediscovery of Warren's Shaft. *Biblical Archaeology Review, 7,* 24-39.

Shiloh, Y. (1984). Excavations at the City of David I, 1978-1982: Interim Report of the First Five Seasons. *Qedem, 19,* 21-24.

Shimron, A. E., & Frumkin, A. (2011). The Why, How and When of the Siloam Tunnel Reevaluated: A Reply to Sneh, Weinberger and Shalev. *Bulletin of the American Schools of Oriental Research, 364,* 53-60. https://doi.org/10.5615/bullamerschoorie.364.0053

Shimron, A. E., Deutsch, Y., Schoch, W. H., & Gutkin, V. (2020). Petrochemistry of Sediment and Organic Materials Sampled from Ossuaries and Two Nails from the Tomb of the Family of the High Priest Caiaphas, Jerusalem. *Archaeological Discovery, 8,* 260-287. https://doi.org/10.4236/ad.2020.83015

Shimron, A., Frumkin, A., Rosenbaum, J., & Porath, Y. (1998). THE CITY OF DAVID WATERWORKS: A Geological and Engineering Overview. In E. Baruch, & G. Ramat (Eds.), *New Studies on Jerusalem. Proceedings of the Fourth Conference* (pp. III-XVI).

Shimron, A., Frumkin, A., Rosenbaum, J., Deutch, Y., & Dvoracek, M. (2000). The Significance of Geological Structures, Cave Sediments and Hydraulic Lime in the Interpretation of the History of the Subterranean Waterworks beneath Ancient Jerusalem. *Geological Survey of Israel, Current Research, 12,* 247-256.

Stager, L E. (1976). *Bulletin of the American Schools of Oriental Research No. 221, Memorial Issue* (pp. 145-158). The University of Chicago Press on Behalf of the American Schools of Oriental Research Stable. https://doi.org/10.2307/1356097

Sulley, H. (1929). *Quarterly Statement of the Palestine Exploration Fund* (p. 124).

Thomas-Keprta, K. L., Clemett, S. J., McKay, D, S., Gibson, E. K., & Wentworth, S. J. (2009). Origins of Magnetite Nanocrystals in Martian Meteorite ALH84001. *Gechimica et Cosmochimica Acta, 73,* 6631-6677. https://doi.org/10.1016/j.gca.2009.05.064

Vincent, L. H. (1911). *Underground Jerusalem*. Discoveries on the Hill of Ophel. Horace Cox Field Office, Windsor House, Bream's Buildingsm, E.C. 40 p. (With Maps, Photos, Sketches and Plates).

Warren, C., & Conder, C. R. (1884). *The Survey of Western Palestine: Jerusalem*. Committee of the Palestine Exploration Fund.

Water Commission Hydrological Service (1970-1998). *Hydrological Year-Books of Israel*. Ministry of Agriculture, Water Commission Hydrological Service.

Zucker, S. B., Khadmy, N. K., Zanvach, R. (2016). From Invagination to Navigation: The Story of Magnetosome-Associated Proteins in Magnetotactic Bacteria. *Protein Science, 25,* 338-351. https://doi.org/10.1002/pro.2827

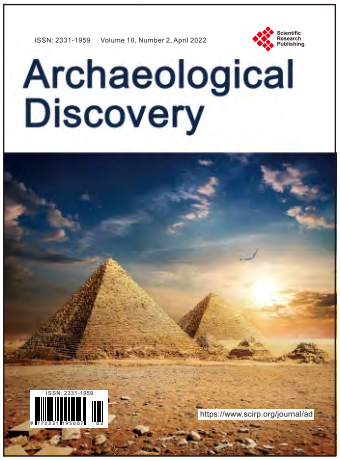

Call for Papers

Archaeological Discovery

ISSN Print: 2331-1959 **ISSN Online: 2331-1967**

https://www.scirp.org/journal/ad

Archaeological Discovery (AD) is an international journal dedicated to the latest advancement in the study of Archaeology. The goal of this journal is to provide a platform for scientists and academicians all over the world to promote, share, and discuss various new issues and developments in different areas of Archaeological studies.

Subject Coverage

All manuscripts must be prepared in English, and are subject to a rigorous and fair peer-review process. Accepted papers will immediately appear online followed by printed hard copy. The journal publishes original papers covering a wide range of fields but not limited to the following:

- Aerial Archaeology
- Archaeological Method and Theory
- Archaeological Science
- Archaeometry
- Art Archaeology
- Environmental Archaeology
- Ethnoarchaeology
- Experimental Archaeology
- Field Archaeology
- Geoarchaeology
- Historical Archaeology
- Island and Coastal Archaeology
- Lithic Studies
- Maritime Archaeology
- Prehistoric Archaeology
- Religious Archaeology
- Social Archaeology
- Underwater Archaeology
- World Archaeology
- Zooarchaeology

We are also interested in: 1) Short reports — 2-5 page papers in which an author can either present an idea with a theoretical background but has not yet completed the research needed for a complete paper, or preliminary data; 2) Book reviews — Comments and critiques, special peer-reviewed issue for colloquia, symposia, workshops.

Website and E-Mail

https://www.scirp.org/journal/ad **E-mail: ad@scirp.org**

What is SCIRP?

Scientific Research Publishing (SCIRP) is one of the largest Open Access journal publishers. It is currently publishing more than 200 open access, online, peer-reviewed journals covering a wide range of academic disciplines. SCIRP serves the worldwide academic communities and contributes to the progress and application of science with its publication.

What is Open Access?

All original research papers published by SCIRP are made freely and permanently accessible online immediately upon publication. To be able to provide open access journals, SCIRP defrays operation costs from authors and subscription charges only for its printed version. Open access publishing allows an immediate, worldwide, barrier-free, open access to the full text of research papers, which is in the best interests of the scientific community.

- High visibility for maximum global exposure with open access publishing model
- Rigorous peer review of research papers
- Prompt faster publication with less cost
- Guaranteed targeted, multidisciplinary audience

Scientific Research Publishing

Website: https://www.scirp.org

Subscription: sub@scirp.org

Advertisement: service@scirp.org